AD-A144 440 NONLINEAR INTERACTION OF TWO NONCOLLINEAR SOUND WAVES 1/2
IN A RECTANGULAR WAVEGUIDE(U) TEXAS UNIV AT AUSTIN
APPLIED RESEARCH LABS J A TEN CATE JUN 84 ARL-TR-84-16
UNCLASSIFIED N00014-75-C-0867 F/G 20/14 NL

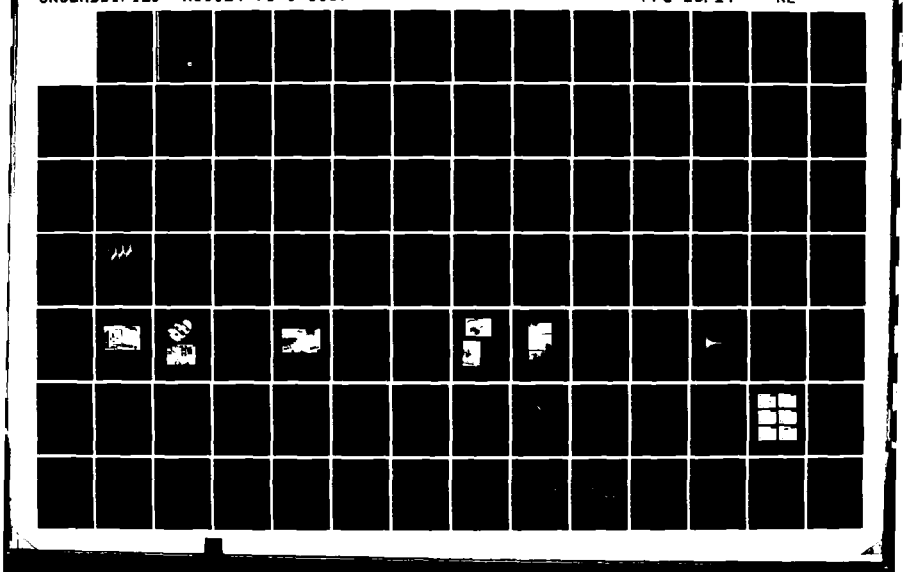

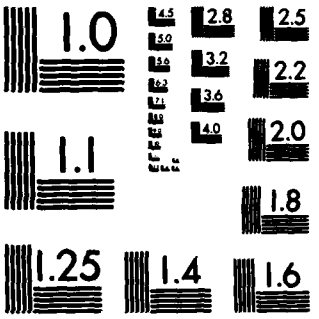

MICROCOPY RESOLUTION TEST CHART
NATIONAL BUREAU OF STANDARDS-1963-A

ARL-TR-84-16

Copy No. 4

NONLINEAR INTERACTION OF TWO NONCOLLINEAR SOUND WAVES IN A RECTANGULAR WAVEGUIDE

James A. Ten Cate

APPLIED RESEARCH LABORATORIES
THE UNIVERSITY OF TEXAS AT AUSTIN
POST OFFICE BOX 8029, AUSTIN, TEXAS 78712-8029

June 1984

Technical Report

Prepared for:

OFFICE OF NAVAL RESEARCH
DEPARTMENT OF THE NAVY
ARLINGTON, VA 22217

UNCLASSIFIED

SECURITY CLASSIFICATION OF THIS PAGE (When Data Entered)

REPORT DOCUMENTATION PAGE	READ INSTRUCTIONS BEFORE COMPLETING FORM
1. REPORT NUMBER	2. GOVT ACCESSION NO. A144440 / 3. RECIPIENT'S CATALOG NUMBER
4. TITLE (and Subtitle) NONLINEAR INTERACTION OF TWO NONCOLLINEAR SOUND WAVES IN A RECTANGULAR WAVEGUIDE	5. TYPE OF REPORT & PERIOD COVERED Technical Report 6. PERFORMING ORG. REPORT NUMBER ARL-TR-84-16
7. AUTHOR(s) James A. Ten Cate	8. CONTRACT OR GRANT NUMBER(s) N00014-75-C-0867
9. PERFORMING ORGANIZATION NAME AND ADDRESS Applied Research Laboratories The University of Texas at Austin Austin, Texas 78713-8029	10. PROGRAM ELEMENT, PROJECT, TASK AREA & WORK UNIT NUMBERS
11. CONTROLLING OFFICE NAME AND ADDRESS Office Naval Research Department of the Navy Arlington, Virginia 22217	12. REPORT DATE June 1984 13. NUMBER OF PAGES 101
14. MONITORING AGENCY NAME & ADDRESS(if different from Controlling Office)	15. SECURITY CLASS. (of this report) UNCLASSIFIED 15a. DECLASSIFICATION/DOWNGRADING SCHEDULE

16. DISTRIBUTION STATEMENT (of this Report)

Approved for public release; distribution unlimited

17. DISTRIBUTION STATEMENT (of the abstract entered in Block 20, if different from Report)

18. SUPPLEMENTARY NOTES

19. KEY WORDS (Continue on reverse side if necessary and identify by block number)

nonlinear acoustics
rectangular waveguides
noncollinear interaction
modulation of sound by sound
suppression of sound by sound

20. ABSTRACT (Continue on reverse side if necessary and identify by block number)

The subject of this report is the nonlinear interaction (in air) of two noncollinear sound waves in a rectangular waveguide. One of the waves is a low frequency, finite-amplitude wave (pump) which travels in the (0,0) mode. The other is a high frequency, small-signal wave which travels in the (1,0) mode. A formula for the modulation, and accompanying suppression, →

DD FORM 1 JAN 73 1473 EDITION OF 1 NOV 65 IS OBSOLETE

UNCLASSIFIED

SECURITY CLASSIFICATION OF THIS PAGE (When Data Entered)

of the small-signal wave by the pump is derived. The modulation depends on the angle of intersection, θ of the two waves because (1) only the velocity component $u\cos\theta$ of the pump convects the small-signal wave, and (2) the two waves have different group velocities (geometric dispersion). Experiments to examine both collinear and noncollinear interaction were performed in a 6.4 m long rectangular waveguide of inside cross-section 70 mm x 38 mm. Waveforms of the frequency modulated small-signal wave were recorded, the suppression of the small-signal primary was measured, and the cyclical variation (in space) of the sum and difference frequency wave amplitudes was examined. Theoretical predictions were generally confirmed.

FOREWORD

This report is a modified version of James A. Ten Cate's M.S. thesis "Nonlinear interaction two noncollinear sound waves in a waveguide." Although the two documents are substantially the same, there are a few differences in emphasis and notation. Note that the word "rectangular" appearing in the report title is not included in the thesis title. The author was enrolled in the Mechanical Engineering Department, The University of Texas at Austin, and his degree was granted in August 1983.

Support for the research came from the Office of Naval Research (ONR) under Contract N00014-75-C-0867 at Applied Research Laboratories, The University of Texas at Austin. Scientific Officer for ONR was L. E. Hargrove.

David T. Blackstock

Supervisor

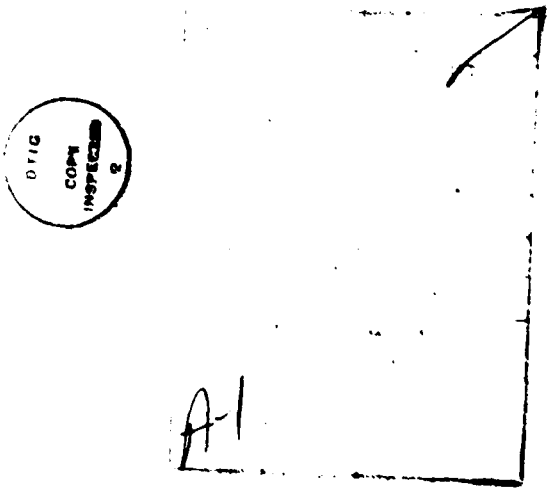

TABLE OF CONTENTS

LIST OF FIGURES

LIST OF IMPORTANT SYMBOLS

a,b	waveguide cross-sectional dimensions (a>b)
B/A	parameter of nonlinearity
c	sound speed
c_o	small-signal sound speed
C_p	specific heat at constant pressure
$D = 2ab/(a + b)$	hydraulic diameter
FM	frequency modulation
f_p, f_w	pump wave frequency, weak wave frequency
f_c	cut-on or cut-off frequency of a waveguide mode
$\hat{i}, \hat{j}$	unit direction vectors in the x-y plane
$J_n(x)$	Bessel function of order n
k_p, k_w	wave number of the pump, weak wave
$\vec{k}_p, \vec{k}_w$	wave vectors of the pump, weak wave
$k_\pm$	wave number at the sum (+), difference (-) frequency
(m,n)	designation of the m,nth waveguide mode
p	acoustic pressure
p_o	ambient pressure
Pr	Prandtl number
r,s	spatial coordinates to describe weak wave propagation
$\hat{r}, \hat{s}$	unit direction vectors in the r-s plane
Δr_{wc}	period of weak wave primary amplitude along r-axis

$\Delta r_{\pm}$	period of sum (+), difference (-) frequency wave amplitude along r-axis
SPL	sound pressure level
t	time
t_o	initial time
u	particle velocity
u_p, u_w	particle velocity of the pump, weak wave
u_{op}, u_{ow}	peak particle velocity of the pump, weak wave
u_+, u_-	particle velocity of the sum, difference frequency waves
u_{wc}	particle velocity of the weak wave primary (central component of the modulated weak wave spectrum)
v_p	speed of propagation of the pump wave in the r direction
x,y,z	cartesian coordinates to describe waveguide geometry
$\bar{x}_p$	shock formation distance for the pump wave
Y_{vbl}, Y_{tbl}	viscous, thermal boundary layer thickness
α_o	(0,0) mode attenuation coefficient
α_1	(1,0) mode attenuation coefficient
$\alpha_{\pm}$	angle the sum (+), difference (-) frequency wave intersects the pump wave
$\beta = 1 + (\gamma-1)/2$	coefficient of nonlinearity for collinear interaction
$\beta_{eff} = \cos\theta + (\gamma-1)/2$	effective coefficient of nonlinearity for noncollinear interaction
γ	ratio of specific heats
ϵ_p, ϵ_w	acoustic Mach number of the pump, weak wave

$\bar{\epsilon}_p$	average pump Mach number (see Eq. (2.38))
ϵ_i	Neumann function
$\eta_\pm$	propagation direction of the sum (+), difference (-) frequency wave
$\Delta\eta_\pm$	period of the sum (+), difference (-) frequency wave amplitude along $\eta_\pm$ axes
η	shear viscosity coefficient
θ	angle between the pump and weak waves
κ	heat conduction coefficient
κ_{mn}	wave number of the (m,n) mode
γ	wavelength
Λ_{mn}	amplitude coefficient of (m,n) mode
$\mu_o = \beta\epsilon_p k_w x$	collinear modulation index
$\mu = \beta_{eff}\,\epsilon_p k_w r$	factor in noncollinear modulation index
μ^{Fenlon}	collinear modulation index obtained from Fenlon's theory
ν	kinematic viscosity
$\sigma_p = \beta\epsilon_p k_p x$	shock formation parameter for the pump wave
$\tau = t - x/c_o$	retarded time (x direction)
$\tau' = t - r/c_o$	retarded time (r direction)
$\Psi = k_p r(1-\cos\theta)/2$	phase factor in Eq. (2.23) and following
ω_p, ω_w	angular frequency of the pump, weak wave
$\omega_\pm = \omega_w \pm \omega_p$	sum (+), difference (-) angular frequencies

CHAPTER 1
INTRODUCTION

The subject of this report is the nonlinear interaction of two noncollinear acoustic wave fields in a rectangular waveguide. One of the fields is that of an intense low frequency wave, the other that of a weak high frequency wave. The two waves propagate down the waveguide in different modes. Traveling in the principal or (0,0) mode, the intense wave modulates the weak wave, which travels in the first oblique or (1,0) mode. The primary purpose of the investigation was to examine the effect of noncollinearity on the modulation. In particular, we wished to examine the vector nature of the nonlinear effect of convection. The investigation was mainly experimental. However, because of the nature of the experiment, a general theoretical study of noncollinear interaction in waveguides was carried out as well.

A. Prelude

One of the distinguishing features of nonlinear acoustics is the nonconstancy of the propagation speed of an intense wave. In particular, the speed $\frac{dx}{dt}$ of a given point on the waveform depends on the value of the particle velocity u at that point. For a plane progressive wave the speed is given by

$$\frac{dx}{dt} = c + u \quad , \tag{1.1}$$

where c is the sound speed. For a gas the (isentropic) relation between c and the acoustic pressure p is

$$c = c_o\left(1 + \frac{p}{p_o}\right)^{(\gamma-1)/2\gamma} \quad , \tag{1.2}$$

where c_o is the small-signal sound speed, p_o is the ambient pressure, and γ is the ratio of specific heats for the gas.* A wave whose amplitude is small enough that $\frac{dx}{dt}$ does not depart noticeably from c_o is called a small-signal wave. A wave for which this departure is significant is called a finite-amplitude wave.

Two effects contribute to the nonconstancy of the propagation speed. The first effect, described mathematically by Eq. (1.2), may be traced to the nonlinearity of the pressure-density relation of the fluid. Because of the nonlinearity, the condensations and rarefactions caused by the wave are accompanied by temperature increases and decreases, respectively. The temperature variations, in turn, cause the local sound speed to vary over the waveform. This effect is purely scalar. The second effect is a vector effect; it is mathematically represented by the presence of u in Eq. (1.1). As a sound wave propagates through a medium, it sets the medium in motion. The moving medium, in turn, adds or subtracts its own speed to the speed of the wave. This effect, called convection, is central to this investigation.

For an ordinary plane progressive wave the two effects may be combined in a single mathematical term. In this case it can be shown[2] that Eq. (1.2) reduces to

$$c = c_o + \frac{\gamma - 1}{2} u \ . \tag{1.3}$$

*For liquids the relation is

$$c = c_o \left[1 + (B/2A)(p/\rho_o c_o^2) \right] ,$$

where B/A is the parameter of nonlinearity and ρ_o is the static density. (See, for example, Blackstock[1] (1962), Section IV).

Substitution in Eq. (1.1) yields

$$\frac{dx}{dt} = c_o + \beta u \quad , \tag{1.4}$$

where

$$\beta = \frac{\gamma - 1}{2} + 1 \quad . \tag{1.5}$$

Both of the effects which contribute to the deviation of the propagation speed from c_o are represented in β, which is called the coefficient of nonlinearity.

The nonconstant propagation speed of an intense wave leads to an interesting well-known result: an intense wave distorts as it travels. For an initially sinusoidal wave the distortion is harmonic; see for example, Thuras, Jenkins, and O'Neil[3] (1935).

In the previous discussion, the propagation and distortion of a solitary, finite-amplitude wave was considered. We now turn our attention to the collinear interaction of two different waves. In particular, we consider the problem of a small-signal wave of high frequency traveling with a finite-amplitude wave of low frequency. In this case the nonlinear effects cause two kinds of distortion. First, ordinary harmonic distortion of the finite-amplitude wave takes place. Second, intermodulation distortion caused by the action of the finite-amplitude wave on the small-signal wave occurs. The second distortion closely resembles that associated with classical frequency modulation. For this reason the interaction effect has been termed the modulation of sound by sound.

The modulation process is illustrated in Fig. 1.1. A source at x=0 generates a low frequency, finite-amplitude wave, Fig. 1.1(a), and a high frequency, small-signal wave, Fig. 1.1(b). Many authors have referred to the former as the "pump" wave and the latter as the "weak" wave. We shall adopt this terminology as

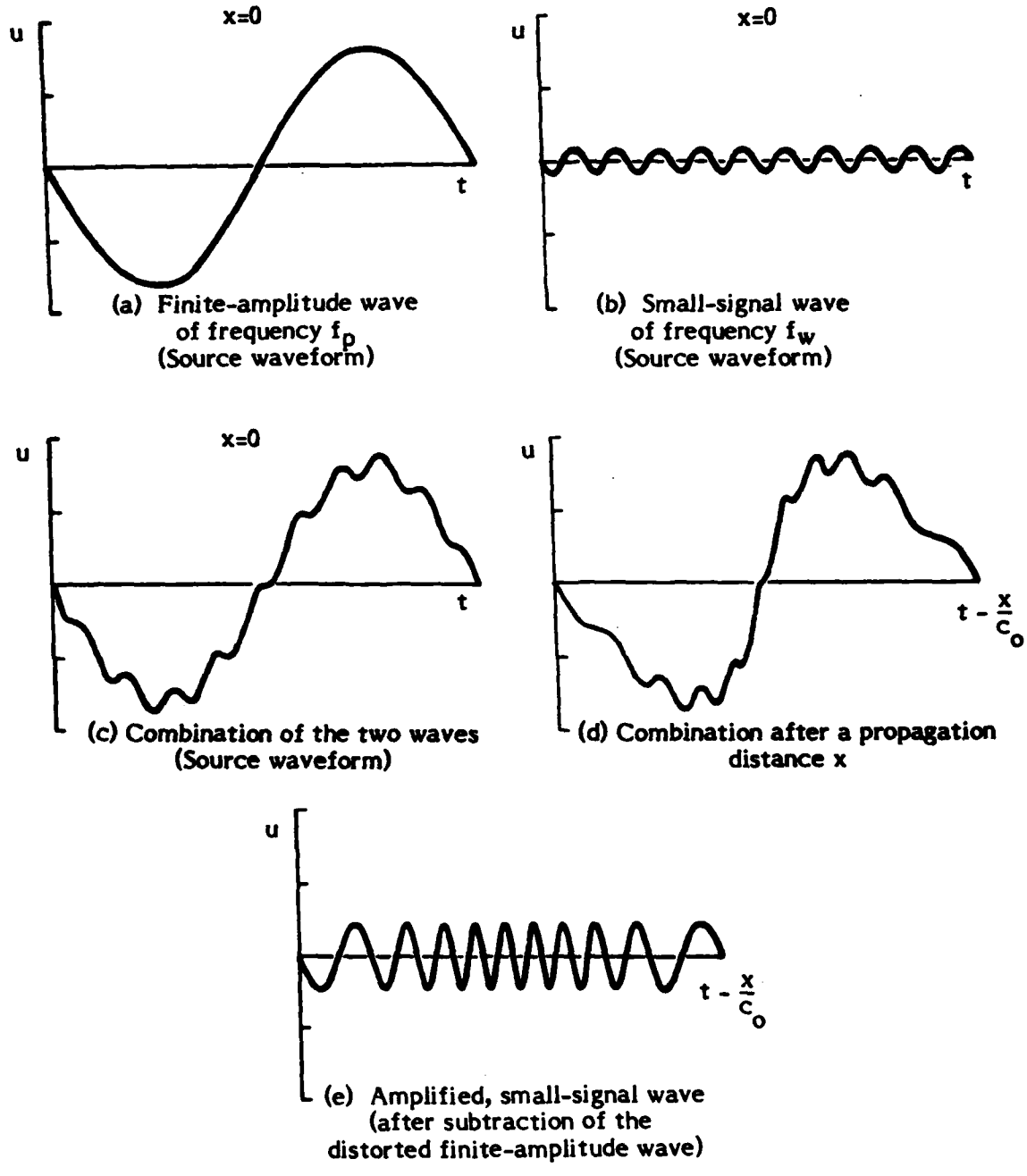

Figure 1.1

Modulation of sound by sound

ARL:UT
AS-84-581
JATC - GA
7 - 9 - 84

well and shall use the subscripts p and w to denote the respective properties of the two waves. Figure 1.1(c) shows the combination of the pump with the weak wave before any propagation has occurred. After the combination wave travels a distance* $\frac{1}{2}\bar{x}_p$, its waveform is that shown in Fig. 1.1(d). Subtraction of the distorted pump waveform from the combination waveform yields the small-signal waveform shown in Fig. 1.1(e). It is apparent that the cycles of the weak wave that traveled with the expansion portions of the pump wave have been stretched while those that traveled with the compression sections have been squeezed. From the figure it is clear that the weak wave has become frequency modulated.

The modulation of sound by sound is particularly interesting when represented in the frequency domain. Besides the two primary components at the frequencies f_p and f_w, other components may be found at frequencies nf_p and $f_w \pm nf_p$, where n is an integer. The set of components at nf_p appears because of harmonic distortion of the pump wave, and the set at $f_w \pm nf_p$ because of intermodulation distortion. Moreover, since the modulation increases as the combination wave propagates, the amplitudes of all of the components vary with distance. In particular, the amplitude of the component at f_w is found to be[4]

$$u_w \propto J_0(\mu_o) \quad ,$$

where J_0 is the Bessel function of order zero. The argument μ_o is called the modulation index and is given by

$$\mu_o = \beta \epsilon_p k_w x \quad ,$$

where $\epsilon_p = u_{op}/c_o$, u_{op} is the amplitude of the pump wave at the source, $k_w = \omega_w/c_o$ is the wave number of the weak wave, and x is the distance propagated. When μ_o is

*$\bar{x}_p$ is the distance the low frequency wave travels before a shock forms.

equal to a zero of the Bessel function, the component at f_w vanishes. This is the process of the suppression of sound by sound. Note that since the suppression depends on the nonlinearity coefficient, a measurement of the suppression allows a determination of the value of the coefficient.

Suppose that we now generalize the interaction phenomenon by allowing the waves to intersect at a nonzero angle θ. Two new effects come into play. First, the relation of the modulation to the nonlinearity coefficient β is more complicated. In particular, only the component of the particle velocity in the direction of the small-signal wave can cause convection of the small-signal wave. This component is $u_p \cos\theta + u_w$, or, since $|u_p| \gg |u_w|$, just $u_p \cos\theta$. On the other hand, the contribution caused by the nonlinearity of the pressure-density relation (see Eq. (1.2)) should not change; the effect is purely scalar. In our analysis, therefore, the effect the finite-amplitude wave has on the small-signal wave depends on an effective coefficient of nonlinearity

$$\beta_{eff} = \frac{\gamma - 1}{2} + \cos\theta \quad . \tag{1.6}$$

For liquids the expression is

$$\beta_{eff} = B/2A + \cos\theta \quad . \tag{1.7}$$

Note that we need only change the factor 1 to $\cos\theta$ in the usual expression for the nonlinearity coefficient to adjust for the effect of convection at an angle θ.

A second effect which distinguishes noncollinear interaction from collinear interaction is geometric dispersion. The two waves do not travel in a given direction, e.g., the propagation direction of the pump wave, with the same speed.

The distortion effect of the pump on a given wavelet of the weak wave is therefore continually changing. Geometric dispersion, which may easily dominate the interaction process, is discussed in detail in Chapter 2.

Despite the changes which occur when the interaction is noncollinear, the modulation and suppression of sound by sound may still be observed. A measurement of the suppression, in fact, allows one to determine the value of β_{eff} and thus to check the validity of Eq. (1.6). An experiment to measure the suppression is the heart of the work reported in this investigation and is described in the next section.

B. Introduction to the experiment

In principle the experiment could have been done either in air or in water. As one may infer from the discussion in the previous section, air was the medium chosen. The primary reason is that the constant component of β_{eff} is much larger for water ($B/2A \doteq 2.5$) than for air ($\frac{\gamma - 1}{2} = 0.2$). In water, therefore, the effect of convection is relatively small. Any measurement of the θ dependence of β_{eff} in water would be extremely difficult.

Various schemes to produce interaction of noncollinear wave fields are possible. The simplest in theory is two infinite plane waves. The main advantage of this arrangement is that no diffraction effects are present. Furthermore, since the two waves are infinite, the region of interaction between the two waves is infinite as well. The disadvantage is that infinite plane waves are quite difficult to obtain in practice.

A more practical approach is to use two collimated sound beams. Indeed, beams have been used in several experiments. One of the earliest was done by Ingard and Pridmore-Brown[5] (1956). They attempted to observe the scattering of sound by sound outside the region of interaction. A difficulty with beams, however,

is that the interaction region is limited by the size of the beams. Diffraction effects frequently prove troublesome as well.

The parametric receiving array offers a third possibility. In this case the pump is a high frequency and the weak wave is a low frequency plane wave of nearly infinite extent. In principle, a very large region of interaction can be obtained. Numerous experiments on the parametric receiving array have been performed in water[6-10] and air[11] and its behavior is well established. Truchard[12] had in fact intended to use the parametric receiving array (in water) to examine the angular dependence of β_{eff} but never reported any results. A disadvantage of the array arrangement is diffraction associated with the beam. Zverev and Kalachev[13] (1970) performed an experiment with a somewhat different arrangement. Using a low frequency intense plane wave as the pump and a high frequency beam as the weak wave, they measured the sum and difference frequency components over an angular range $-\pi/2 < \theta < \pi/2$. Their contribution to the theory of noncollinear modulation of sound by sound is discussed in Section C.

A completely new idea was considered by Essert[14] (1981). He intended to confine two waves in a circular tube. The first wave would travel straight down the tube in the principal mode. The second wave would propagate in a bouncing mode and would thus interact at an angle with the first wave. The primary advantage is that the effects of diffraction, which play a strong role in beam experiments, play no role in a tube. Another advantage is that the region of interaction is limited only by the length of the tube. The main disadvantage is that the bouncing wave suffers focusing at the center of the tube. Indeed, the phase distortion caused by the focusing affected the interaction so much that Essert decided to concentrate on the focusing phenomenon instead and therefore never carried out an interaction experiment.

The use of a waveguide for the interaction experiment was, however, basically sound. Rudnick suggested a solution of the focusing problem: use a rectangular rather than circular waveguide.[15] This scheme, which has numerous advantages, was the one chosen for this investigation. The interaction of the two waves is shown in Fig. 1.2. The finite-amplitude wave travels in the principal or

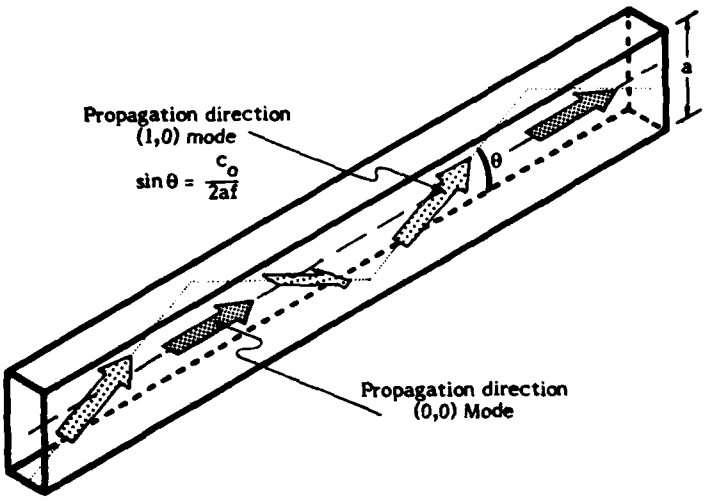

Figure 1.2

Propagation of (0,0) and (1,0) modes in a waveguide (f=frequency)

ARL:UT
AS-84-582
JATC - GA
7 - 9 - 84

(0,0) mode (i.e., an ordinary plane wave) and the small-signal wave travels in the (1,0) mode. The angle of intersection between the two waves may be altered simply by varying the frequency of the (1,0) mode. See the equation in the figure. One remaining question needs to be answered: Is this experiment really equivalent to one with infinite plane waves? That is, do the reflections by the walls of the

waveguide introduce any new effects? Since the wave being reflected is small-signal, the incident and reflected components should not interact to generate nonlinear effects. Furthermore, although the mode may be viewed as the superposition of two wave fields, the interaction, which is governed by the value of $\cos\theta$, is the same for both wave fields.

C. Historical survey

At this point, it is of interest to examine previous studies--both collinear and noncollinear--of the nonlinear interaction of two waves. We pay most attention to those accounts which deal with modulation of sound by sound. Our survey also emphasizes the experimental work rather than the theoretical. Numerous experiments in all types of media have been reported. Most of the experiments deal with either perpendicular or collinear interaction of two waves. Nearly all of the collinear wave experiments[4,21,22,28-31] were designed to examine some aspect of the modulation or suppression of sound by sound. Certain studies of perpendicularly interacting waves in liquids[18-20] had a practical side, namely the measurement of B/2A.* Other experiments[5,23] were done mainly to study the scattering of sound by sound. Finally, studies of interactions at other angles[6-10,13,32] are considered at the end of this section.

Studies of the nonlinear interaction of two waves span an extensive period in the literature. In fact, accounts of the phase (or frequency) modulation of one wave by another were published as early as the 1950's. Pimonow[16] (1954) related a fascinating account of various qualitative modulation experiments. He reported and

*Since $\cos\theta = 0$ for perpendicular interaction, β_{eff} reduces to the single term, B/2A.

discussed the observation of Tartini tones* as well as the modulation of a standing ultrasonic wave field by a strong, low frequency wave; he also suggested a design for an invisible, gaseous microphone. Mikhailov[18] (1953) attempted to observe a similar modulation in glycerin by an experiment with two perpendicularly interacting waves. His apparatus, however, was inadequate and he was unable to obtain the results he expected. Gorelik and Zverev[19] (1957) performed a perpendicular interaction experiment in water and managed to successfully observe and study the phase modulation of a small-signal plane wave. Other liquids (ethyl alcohol and a saline solution) were investigated by Zverev and Kalachev[20] (1959), who also gave a brief theoretical analysis of the perpendicular interaction between the two waves. Indeed, their paper is one of the first published accounts in which the classical frequency modulation (FM) solution (as it applies to the interaction problem) is presented. Moreover, the authors determined--with moderate success--the constant B/2A for each liquid in which the experiment was performed.

Quantitative modulation experiments have also been done in air and in solids. With hopes of developing a new microphone calibration technique, Mrass and Brinkmann[4] (1964) used two collinear waves to observe and study the modulation of a weak high frequency wave by an intense low frequency wave in air. Their study was both theoretical and experimental. Their theoretical analysis is much more detailed than that of Zverev and Kalachev.[20] For example, the authors used their theory to predict the entire frequency spectrum of the modulated wave. The modulation of sound by sound was also detected in a solid (lead molybdate) by

*The curious reader should see pp. 9-10 in Beyer's book[17] for an interesting discussion of Tartini tones.

Rouvaen, Bridoux, Moriamez, and Torguet[21] (1973). More recently, Aksenov and Sherbakov[22] (1980) described the utilization of the phenomenon in the same solid for the design of an acoustooptic correlator.

While the early examinations of the modulation of sound by sound were being carried out, articles on a related topic, the scattering of sound by sound, began to appear. While the observation point for the modulation of sound by sound is always within the interaction region, the observation point for the scattering of sound by sound is outside it. The earliest and perhaps the most controversial of the scattering papers is that of Ingard and Pridmore-Brown[5] (1956) in which the authors deal with the scattering between two perpendicular waves. Their measurements sparked a controversy which raged for nearly a decade and has recently been renewed.* A multitude of related papers followed, including one which presented a most important discovery--Westervelt's parametric array (1960).[25] These papers are too numerous to mention here; the interested reader should consult Beyer[17] for an excellent review.

Despite the many studies involving modulation of sound by sound up to this point, in none is there any mention of the application to suppression (or absorption†) of sound by sound. Fenlon[27] (1972) derived the exact expression (more general than that presented by Mrass and Brinkmann[4]) for the spectrum resulting from a multi-frequency, finite-amplitude source of collinear waves. Although he

*See, for example, Trivett and Rogers[23] (1982) and Westervelt[24] (1983). It appears the issue is still not settled.

†The term "absorption" of sound by sound was coined by Westervelt.[26] Most authors have preferred the term "suppression," however, because no energy is really lost in the interaction.

did not develop the theory with the suppression of sound by sound in mind, his results can easily be applied to the problem. In fact, his theory shows that the ordinary FM description presented by Mrass and Brinkmann is too simple. Fenlon's theory was first applied to the suppression of a weak, high frequency wave by an intense low frequency wave by Moffett, Konrad, and Carlton[28] (1978). These authors indicate that suppression was observed as early as 1972. Schaffer[29] (1975) was the first to observe the suppression of sound by sound in air. He performed experiments in a progressive plane wave tube and achieved weak wave suppressions of up to 40 dB.* An interesting comparison between the predictions based on FM theory and Fenlon's solution is included in Schaffer's discussion. Both predictions are also compared with experimental results. Willshire[31] (1977) reversed the frequencies of the pump and weak wave. That is, he considered the modulation of a low frequency, small-signal wave by an intense, high frequency wave. He confirmed the prediction based on Fenlon's solution that an intense, high frequency wave simply does not greatly affect a low frequency wave. The strongest modulation which can occur is of a high frequency wave by a low frequency wave, regardless of their respective amplitudes.

Next we consider investigations of interaction at angles other than 0° or 90°. The first experiment and analysis of oblique interaction in air was reported by Date and Tozuka[11] (1968), who were interested in the design of a parametric directional microphone. Although they were concerned with noncollinear interaction, they used the expression $\frac{\gamma+1}{2}$ for β_{eff} instead of $\cos\theta + \frac{\gamma-1}{2}$. Zverev and Kalachev[13] (1970), who disagreed with the expression for β_{eff} used by Date and Tozuka, gave the first detailed theory of the noncollinear modulation of sound by

*In a recent repeat of this experiment, Gong, Zhu, and Du[30] (1979) achieved as much as 47 dB suppression of the small-signal wave.

sound. In particular, the authors derived a phase modulation index for the modulated wave and also obtained expressions for the directivity of the sum and difference frequency waves. The directivity predictions were experimentally verified by the authors. Pridham[32] (1974) also developed a theory for noncollinear interaction; it is similar to that presented by Zverev and Kalachev.

During the same period, two other topics, the parametric receiving array[6-10] and the interaction of noise with a finite-amplitude tone,[26,29,33-37] were being investigated. Although both topics involve collinear and noncollinear interactions, they are only remotely related to our investigation. We mention them only for completeness.

Even though the suppression of sound by sound has become a well-known phenomenon, no experiments of noncollinear suppression, either in water or air, have been reported. Our investigation is thus a logical continuation of the work of Zverev and Kalachev and of Schaffer.

D. Scope of the investigation

The remaining chapters are divided as follows. Chapter 2 contains a theoretical development of the noncollinear suppression of sound by sound in a waveguide and an analysis of implications of that theory. Chapter 3 comprises a discussion of experimental apparatus and preliminary tests. The main experimental results are presented in Chapter 4. Conclusions and a final discussion make up the final chapter.

CHAPTER 2
THEORY

In this chapter a theory for modulation of a weak, high frequency plane wave by an intense, low frequency plane wave is described. The two waves are not necessarily collinear. First, the interaction is considered to take place in a free field. After collinear interaction is reviewed, the theory is extended to cover noncollinear interaction. Of particular interest is the effect of noncollinearity on suppression of sound by sound. After a general discussion of rectangular waveguides, the effect of containing the two fields in a waveguide is considered. The addition of tube wall attenuation and dispersion in the theory concludes the chapter.

Throughout the analysis the following limitations, assumptions, and nomenclature apply. It has already been noted that the interaction is between a finite-amplitude wave called the pump and a small-signal wave called the weak wave. The analysis is simplified if we assume that the angular frequency of the pump wave (ω_p) is much less than that of the weak wave (ω_w). Finally, the results are valid only if no shocks have formed.

A. Collinear interaction

In this section we review the theory for collinear interaction of two progressive plane waves. The equation governing collinear interaction of plane waves in a lossless fluid is the ordinary nonlinear wave equation,[1]

$$\frac{\partial u}{\partial t} + c_o \frac{\partial u}{\partial x} + \beta u \frac{\partial u}{\partial x} = 0 \quad . \tag{2.1}$$

The general solution satisfying the boundary condition u(0,t) = f(t) is

$$u(x,t) = f\left(t - \frac{x}{c_o + \beta u}\right) \quad . \tag{2.2}$$

Hereafter, we shall refer to Eq (2.2) as the Poisson solution (although the medium assumed by Poisson was one for which $\beta = 1$). If $\left|\frac{\beta u}{c_o}\right| << 1$, the argument of f( ) may be approximated by $t - \frac{x}{c_o} + \frac{\beta u x}{c_o^2}$. Thus, an approximate Poisson solution is

$$u(x,\tau) = f\left(\tau + \frac{\beta u x}{c_o^2}\right) \quad , \tag{2.3}$$

where $\tau = t - \frac{x}{c_o}$ is the retarded time.

The approximate Poisson solution is now applied to the problem of collinear interaction of two waves. Given the boundary condition

$$u(0,t) = u_{op} \sin \omega_p t + u_{ow} \sin \omega_w t \ , \tag{2.4}$$

the solution is

$$u(x,\tau) = u_{op} \sin \omega_p\left(\tau + \frac{\beta u x}{c_o^2}\right) + u_{ow} \sin \omega_w\left(\tau + \frac{\beta u x}{c_o^2}\right) \quad . \tag{2.5}$$

The first term in Eq. (2.5) may be roughly considered to represent the pump wave u_p, the second term the weak wave u_w.

Two well-known results may be obtained from Eq. (2.5) by making simple approximations. To begin, we consider just the first term of the equation. Since $u_{op} << u_{ow}$, the factor u which appears in the argument of the sine function may be approximated by u_p and the solution becomes

$$u_p = u_{op} \sin \omega_p \left(\tau + \frac{\beta u_p x}{c_o^2}\right) \quad . \tag{2.6}$$

By well-known manipulations,[1] Eq. (2.6) may be solved for u_p to obtain

$$u_p(x,\tau) = u_{op} \sum_{n=1}^{\infty} \frac{2}{n\sigma_p} J_n(n\sigma_p) \sin \omega_p \tau \ , \tag{2.7}$$

where $\sigma_p = \beta \epsilon_p k_p x$, $\epsilon_p = \frac{u_p}{c_o}$ and $k_p = \frac{\epsilon_p}{c_o}$. Equation (2.7) is the Bessel-Fubini solution.[2]

The second well-known result may be obtained from the second term of Eq. (2.5). In this case the somewhat cruder approximation $u = u_{op} \sin \omega_p \tau$ is used in the argument of the sine function. We obtain

$$u_w(x,\tau) = u_{ow} \sin \left[\omega_w \tau + \mu_o \sin \omega_p \tau \right] , \tag{2.8}$$

where

$$\mu_o = \beta \epsilon_p k_w x \ . \tag{2.9}$$

Equation (2.8) is the expression for a frequency modulated wave. The quantity μ_o is the modulation index and depends on u_p and ω_w and not u_w or ω_p. To find the spectrum of the signal, it is convenient to express Eq. (2.8) in complex form. The equation becomes

$$u_w = u_{ow} \, \mathrm{Im} \left[e^{i\omega_w \tau} \ e^{i\mu_o \sin \omega_p \tau} \right] \ . \tag{2.10}$$

Using the identity

$$e^{i\mu_o \sin \omega_p \tau} = \sum_{n=-\infty}^{\infty} J_n(\mu_o) \, e^{in\omega_p \tau} \ , \tag{2.11}$$

we obtain

$$u_w = u_{ow} \sum_{n=-\infty}^{\infty} J_n(\mu_o) \sin(\omega_w + n\omega_p)\tau \quad , \tag{2.12}$$

or, alternatively,

$$u_w = u_{ow} \left\{ J_0(\mu_o) \sin \omega_w \tau \right.$$

$$\left. + \sum_{n=1}^{\infty} J_n(\mu_o) \left[\sin (\omega_w + n\omega_p)\tau + (-1)^n \sin (\omega_w - n\omega_p)\tau \right] \right\} \quad . \tag{2.13}$$

The first term represents the primary or central frequency component of the modulated weak wave. Hereafter, we shall denote this component as u_{wc}. The other terms represent the sidebands. The amplitude of the primary component is easily seen to be proportional to $J_0(\mu_o)$. When the value of μ_o is equal to a zero of the Bessel function, the amplitude of this component is zero. The process just described is, as noted in Chapter 1, the suppression of sound by sound. Numerous experiments[4,21,28-30] have confirmed this prediction.

An alternative approach to the problem may be obtained from the complete solution for an N frequency source excitation--N an integer--given by Fenlon.[27] His solution may be adapted to our problem by letting N=2 and taking $u_{op} << u_{ow}$. Fenlon's solution then reduces to the sum of two series, one for the pump and one for the weak wave. The series for the pump is Eq (2.7), the Bessel-Fubini solution. The series for the weak wave is Eq. (2.12), except that the modulation index is

$$\mu^{\text{Fenlon}} = \mu_o + n\beta\epsilon_p k_p x \quad . \tag{2.14}$$

In other words, the "Fenlon solution" for the modulated weak wave is

$$u_w^{\text{Fenlon}} = u_{ow} \sum_{n=-\infty}^{\infty} J_n \left[\mu_o (1 + n \frac{\omega_p}{\omega_w}) \right] \sin (\omega_w + n\omega_p)\tau \quad . \qquad (2.15)$$

For the case $u_{op} >> u_{ow}$, this solution is exact.

The FM solution may be obtained from Eq. (2.15) if we assume $\omega_p << \omega_w$. However, by making this assumption, we lose the term that represents the modulation of the pump wave by the weak wave. Thus, even though both solutions predict identical amplitudes for the primary component of the modulated weak wave, the FM solution fails to accurately predict the amplitudes of the sidebands. In spite of its shortcoming, the FM solution is still an attractive description. The analysis which leads to it makes the physical process quite clear; the same cannot be said of Fenlon's solution.

B. Noncollinear interaction

Now extend the theory to noncollinear interaction. Two modifications come into play. First, the expression for β, the nonlinearity coefficient, must be changed. Only the component of the particle velocity of the pump in the direction of the weak wave contributes to convection of the latter. In particular, the coefficient is expected to have the form given by Eq. (1.6). Second, geometric dispersion is introduced. The propagation speeds of two noncollinear waves in a given direction are different. Geometric dispersion was only briefly mentioned in the previous chapter. We now examine it in more detail.

Figure 2.1 shows the effect of geometric dispersion in the cases of collinear and noncollinear interaction. Spatial waveforms of the two waves at two separate times are shown for each case. Focus attention on the outlined section of

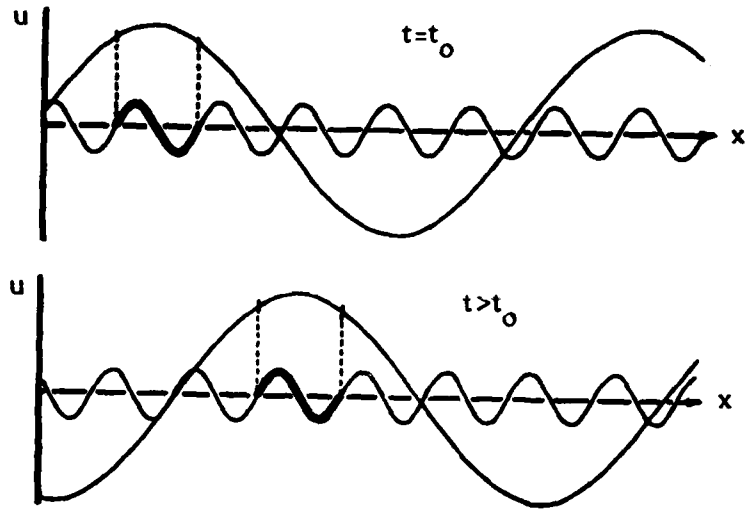

(a) Collinear interaction -- no geometric dispersion

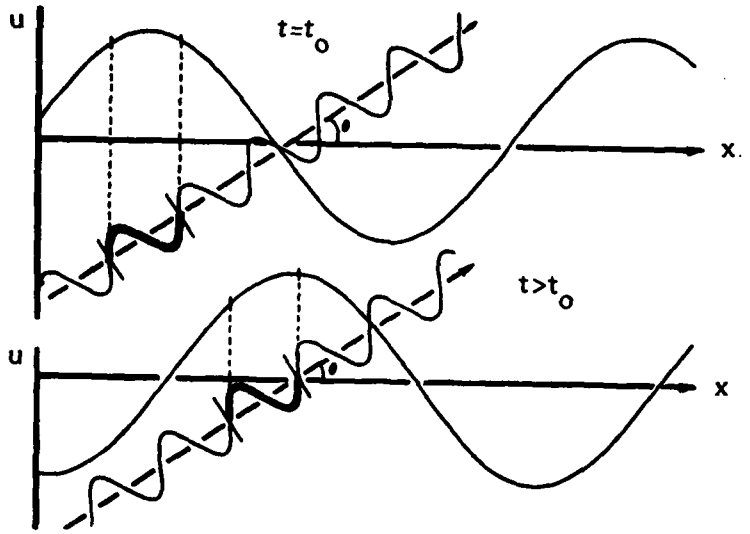

(b) Noncollinear interaction -- geometric dispersion

Figure 2.1

Comparison of dispersive effects
in collinear and noncollinear interaction

ARL:UT
AS-84-583
JATC - GA
7 - 9 - 84

the high frequency wave. In the collinear case, Fig. 2.1(a), it is apparent that this section always travels with the same portion of the low frequency waveform. The two waves are phase-locked and there is no geometric dispersion. However, the same is not true in the noncollinear case, Fig. 2.1(b). The outlined section slides back along the axis of the low frequency wave. In other words, the propagation speed of the high frequency wave in the direction of the low frequency wave is less than that of the low frequency wave.

Geometric dispersion and the change in the form of β may now be incorporated in the theory. Our analysis will be similar to the one which led us to the FM solution. Figure 2.2 shows the coordinate systems used in the analysis. The

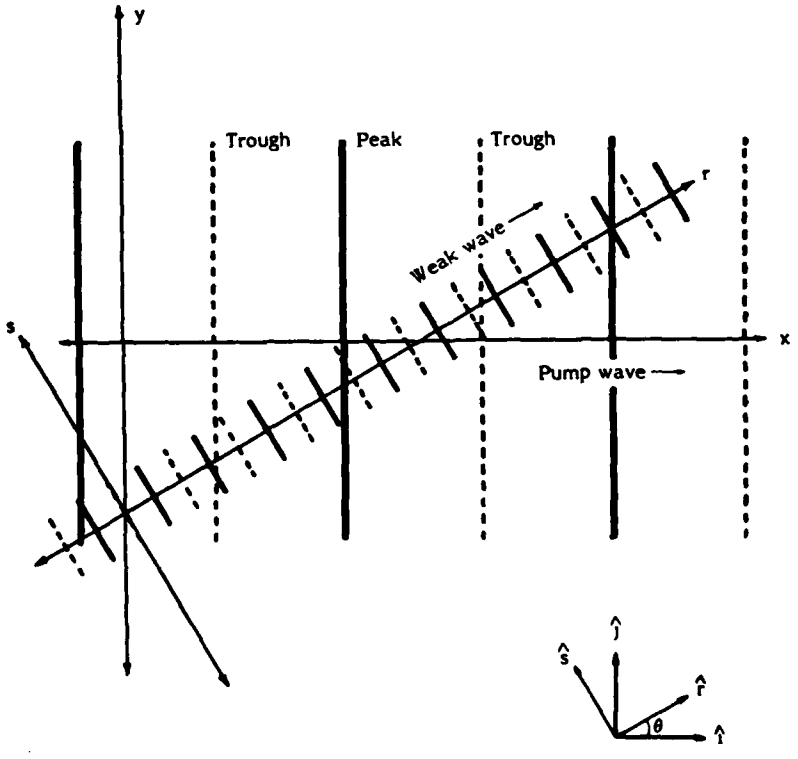

Figure 2.2

Interaction geometry
and coordinate systems

ARL:UT
AS-84-584
JATC - GA
7 - 9 - 84

unit direction vectors in the x-y plane are $\hat{\imath}$ and $\hat{\jmath}$; those in the rotated reference plane are $\hat{r}$ and $\hat{s}$. The pump wave travels in the x direction, the weak wave in the r direction, that is, the wave vectors are $\vec{k}_p = \frac{\omega_p}{c_o}\hat{\imath}$ and $\vec{k}_w = \frac{\omega_w}{c_o}\hat{r}$.

The analysis begins with a "Poisson-like" solution for the weak wave. Because a given wavelet of the weak wave is not always affected by the same part of the pump (see Fig. 2.1(b)), the distorting effect of the pump on the wavelet is an integrated effect. The Poisson solution becomes

$$u_w = u_{ow} \sin \omega_w \left(t - \int_0^r \frac{dr'}{v_p}\right) \quad , \tag{2.16}$$

where v_p is the speed of propagation, due to the presence of the pump, in the r direction,

$$v_p = c_o + \beta_{eff} u_p \quad ,$$

and $\beta_{eff} = \cos\theta + (\gamma-1)/2$. The approximate Poisson solution for the weak wave may thus be expressed as

$$u_w(r,\tau') = u_{ow} \sin \omega_w \left(\tau' + \frac{\beta_{eff}}{c_o^2}\int_0^r u_p \, dr'\right) \quad , \tag{2.17}$$

where $\tau' = t - \frac{r}{c_o}$. Note that $x = r\cos\theta$. Thus when the approximation

$$u_p = u_{op} \sin(\omega_p t - k_p x)$$

$$= u_{op} \sin(\omega_p t - k_p r \cos\theta) \tag{2.18}$$

is substituted into Eq. (2.17), the result is

$$u_w(r,\tau') = u_{ow}\sin\omega_w\left[\tau' + \frac{\beta_{eff}u_{op}}{c_o^2}\int_0^r \sin\left(\omega_p\tau' + k_p r'(1-\cos\theta)\right)dr'\right] \quad . \quad (2.19)$$

If the integration is performed, with τ' constant, the solution is

$$u_w(r,\tau') = u_{ow}\sin\left[\omega_w\tau' + \left(\mu\frac{\sin\Psi}{\Psi}\right)\sin(\omega_p\tau' + \Psi)\right] , \quad (2.20)$$

where

$$\Psi = \frac{1}{2}k_p r(1-\cos\theta) \quad (2.21)$$

and

$$\mu = \beta_{eff}\epsilon_p k_w r \quad . \quad (2.22)$$

We shall call $\frac{\sin\Psi}{\Psi}$ the geometric dispersion factor.

Like Eq. (2.8), Eq. (2.20) represents a frequency modulated wave. This time, however, the modulation index is $\mu\frac{\sin\Psi}{\Psi}$. If a spectral analysis of Eq. (2.20) is performed, the result is

$$u_w(r,\tau') = u_{ow}\sum_{n=-\infty}^{\infty} J_n\left(\mu\frac{\sin\Psi}{\Psi}\right)\sin\left[(\omega_w + n\omega_p)\tau' + n\Psi\right] \quad . \quad (2.23)$$

Except for the extra phase term $n\Psi$ and the form of the modulation index, Eq. (2.23) is quite similar to Eq. (2.12). Indeed, in the limit as $\theta \to 0$, Eq. (2.23) reduces to Eq. (2.12).

C. Comparisons and discussion

The effects of noncollinearity on the modulation--the change of β to β_{eff} and the introduction of the geometric dispersion factor $\frac{\sin\Psi}{\Psi}$--are now discussed, first for the central component of the weak wave spectrum and then for the sidebands.

1. Primary component

Let the primary, or central, component n=0 of the modulated weak wave spectrum be denoted u_{wc},

$$u_{wc}(r,\tau') = u_{ow} J_0\left(\mu \frac{\sin\Psi}{\Psi}\right) \sin(\omega_w \tau' + \Psi) \quad .$$

The relative magnitude of this signal is

$$\left|\frac{u_{wc}}{u_{ow}}\right| = \left| J_0\left(\mu \frac{\sin\Psi}{\Psi}\right)\right| \quad . \tag{2.24}$$

An analysis of Eq. (2.24) shows how different noncollinear modulation is from collinear modulation. In the case of collinear modulation the modulation index does not depend on k_p and varies linearly with r (see Eq. (2.22)). The behavior of the index for noncollinear modulation is quite different. Notably, the index does depend on k_p; furthermore, although the factor $\frac{\mu}{\Psi}$ does not vary with distance, the remaining term $\sin\theta$ does. The magnitude of the primary is thus periodic in r with period

$$\Delta r_{wc} = \frac{2\pi}{k_p(1 - \cos\theta)} \quad , \tag{2.25}$$

where Δr_{wc} is the distance between each successive maxima or minima of the primary signal. At certain values of r, $\sin\Psi = 0$ and no suppression of the signal may be expected. At other values of r, $\sin\Psi = 1$ and a maximum suppression* of the signal may be found. This behavior is shown in Fig. 2.3(a).

*Complete suppression, although theoretically possible, could not be achieved with our experimental appartus. Details may be found in Chapter 4.

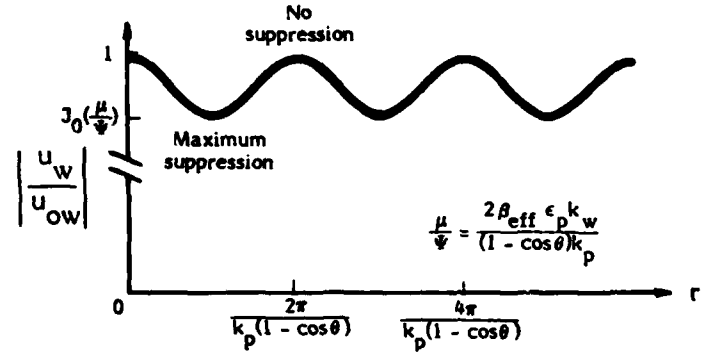

(a) Amplitude of component at frequency f_w

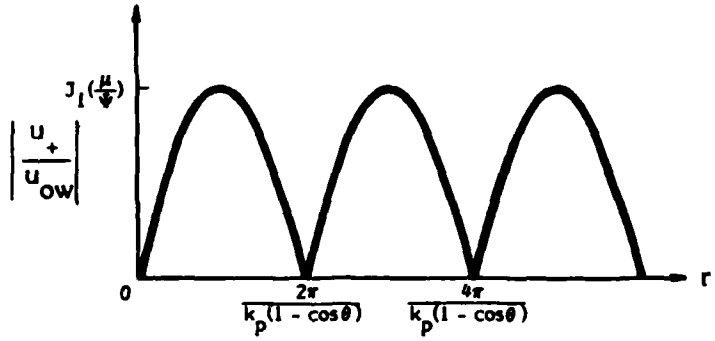

(b) Amplitude of component at sum frequency

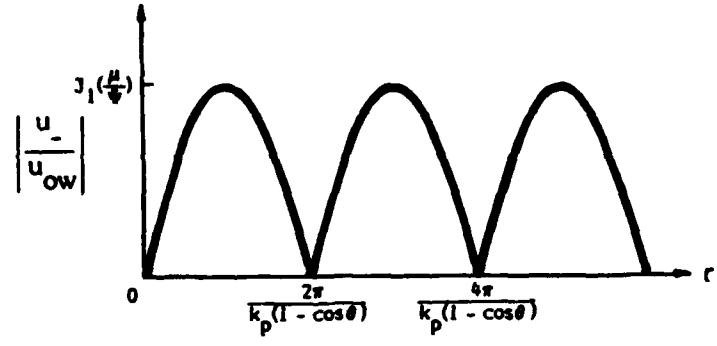

(c) Amplitude of component at difference frequency

Figure 2.3

The effect of geometric dispersion on the weak wave and the sum and difference frequency waves

ARL:UT
AS-84-585
JATC - GA
7 - 9 - 84

2. Sum and difference frequency components

Next consider the first two sidebands of the modulated weak wave spectrum, which are represented by the $n = \pm 1$ terms of Eq. (2.23),

$$\frac{u_{\pm}}{u_{ow}} = J_1\left(\mu \frac{\sin\Psi}{\Psi}\right) \sin\left[(\omega_w \pm \omega_p)\tau' \pm \Psi\right] \quad . \tag{2.26}$$

The (+) sign denotes sum frequency, the (-) sign difference frequency. Although the modulation index is the same as that for the central component, the Bessel function is now J_1. The presence of the phase factor Ψ, because of its dependence on r, implies that the directions of propagation of the sum and difference frequency waves are not along the r-axis. However, because of our tacit assumption that $\omega_w >> \omega_p$, the angles made with the r-axis are small. Details may be found in Appendix A.

The amplitudes of the sum and difference frequency waves are

$$\left|\frac{u_{\pm}}{u_{ow}}\right| = \left|J_1\left(\mu \frac{\sin\Psi}{\Psi}\right)\right| \quad . \tag{2.27}$$

It may be seen that the amplitudes of the these signals are also periodic in r with period

$$\Delta r_{\pm} = \frac{2\pi}{k_p(1 - \cos\theta)} \quad . \tag{2.28}$$

At values of r such that $\sin\Psi = 0$, the sum and difference frequency components vanish. At values such that $|\sin\Psi| = 1$, the amplitudes of the components are maximum. The amplitudes of all three components as functions of r may be compared in Fig. 2.3. Note that the sum and difference frequency magnitude plots are identical. This is not an unexpected result: a symmetric spectrum about ω_w is

an identifying feature of FM theory. Furthermore the sideband amplitudes are maximum whenever the amplitude of the primary component is minimum, and they are zero whenever the primary amplitude is maximum. This result is also not unexpected.

We have already noted that the application of Fenlon's exact solution to the problem of two collinearly interacting waves shows that the FM description of the problem is too simple. Although the FM description accurately predicts the behavior of the primary component of the weak wave, it does not do as well with the sidebands. This fact was experimentally demonstrated by Schaffer. The same holds true for noncollinear interaction. An alternative formulation of the noncollinear interaction problem given by Hamilton[38] may be found in Appendix B. Although his analysis is limited to weak waves, his results indicate that the amplitudes of the sum and difference frequency components do not behave the same. See Eq. (B.9). If $\omega_w >> \omega_p$, however, Hamilton's results do reduce to those of FM theory. Predictions from both theories are compared experimentally in Chapter 4.

D. Waveguides

As explained in Chapter 1, noncollinear interaction is studied here by observing the interaction of a (0,0) and (1,0) mode in a rectangular waveguide. The (0,0) mode is the pump, the (1,0) mode the weak wave. A brief review of propagation in waveguides is thus in order.

Suppose we wish to examine the propagation of a small-signal wave in the rectangular waveguide represented in Fig. 2.4. If the walls of the waveguide are rigid, the normal component of the particle velocity is zero and the pressure

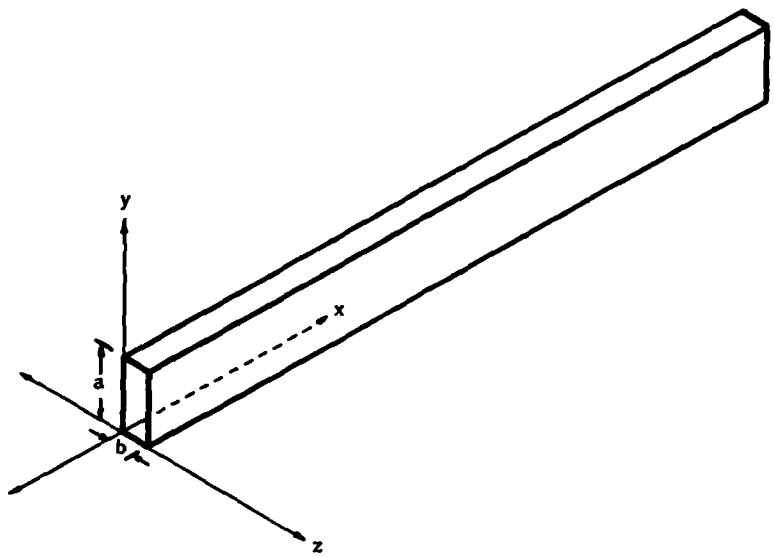

Figure 2.4
Waveguide geometry

ARL:UT
AS-84-586
JATC - GA
7 - 9 - 84

amplitude maximum at each wall. With these boundary conditions the solution of the wave equation

$$\nabla^2 p - \frac{1}{c_o^2} \frac{\partial^2 p}{\partial t^2} = 0$$

is

$$p = \sum_{m,n} p_{mn} \ ,$$

where the modes p_{mn} are given by

$$p_{mn} = A_{mn} \cos \frac{m\pi y}{a} \cos \frac{n\pi z}{b} e^{i(\omega t - \kappa_{mn} x)} \qquad (2.29)$$

and

$$\kappa_{mn} = \sqrt{\left(\frac{\omega}{c_o}\right)^2 - \left(\frac{m\pi}{a}\right)^2 - \left(\frac{n\pi}{b}\right)^2} \quad .$$

The amplitudes Λ_{mn} are to be determined from source conditions.

For true propagation the wave number κ_{mn} must be real, that is,

$$\frac{\omega}{c_o} \geq \sqrt{\left(\frac{m\pi}{a}\right)^2 + \left(\frac{n\pi}{b}\right)^2}$$

or

$$f \geq f_c = \frac{c_o}{2}\sqrt{\left(\frac{m}{a}\right)^2 + \left(\frac{n}{b}\right)^2} \quad . \tag{2.30}$$

The cut-off (or cut-on) frequency f_c of the principal mode (m=n=0) is identically zero. Sound therefore propagates in this mode at any frequency. If either m or n is not equal to zero, $f_c>0$. Propagation occurs in this case only if the frequency is above the cut-on frequency. Below cut-on, κ_{mn} is imaginary and the wave is exponentially damped and dies quickly. Such a mode is called evanescent.

Whether a particular mode is excited in a waveguide is determined by the source conditions. If a source condition is given as

$$p = f(0,y,z) \quad ,$$

then the coefficients Λ_{mn} in Eq. (2.29) are given by[39]

$$\Lambda_{mn} = \frac{\epsilon_m \epsilon_n}{ab}\int_0^b \int_0^a f(0,y,z)\, dy\, dz \quad ,$$

where ϵ_i is the Neumann function $\epsilon_i = \begin{cases} 1 & i=0 \\ 2 & i>0 \end{cases}$. With appropriately chosen source conditions, certain Λ_{mn} vanish, that is, the corresponding modes are not excited. The source conditions used in our experiments are discussed in Chapter 3.

Propagation of the (1,0) mode in a waveguide is especially important in our investigation and thus merits some discussion. Figure 2.5(a) shows the pressure field of the (1,0) mode at one given instant of time. Note that the z-axis is the pressure axis. The solid and dashed lines projected on the plane $z = P_o$ are the wavefront peaks and troughs of the two waves, respectively. However, since the plot is frozen in time, it is difficult to see the propagation direction of the mode. The projection of the wavefronts onto the plane $z = P_o$ is shown separately in Fig. 2.5(b); the direction of propagation is the ray perpendicular to the wavefronts. The angle of intersection between the propagation direction of the (1,0) mode and the (0,0) mode (the x-axis) is thus given by

$$\sin\theta = \frac{\lambda}{2a}$$

or

$$\theta = \arcsin\left(\frac{c_o}{2af_w}\right) . \tag{2.31}$$

Measurements of the pressure fields in the waveguide are made along its length, i.e., the x-axis in Fig. 2.5. The expressions describing the modulation of the weak wave, are however, expressed in terms of r. To put them in terms of x, use the relation $r = \frac{x}{\cos\theta}$. The modulation index becomes

$$\mu \frac{\sin\Psi}{\Psi} = \frac{2\beta_{eff}\epsilon_p k_w}{k_p(1-\cos\theta)} \sin\left[\frac{k_p x (1-\cos\theta)}{2\cos\theta}\right] . \tag{2.32}$$

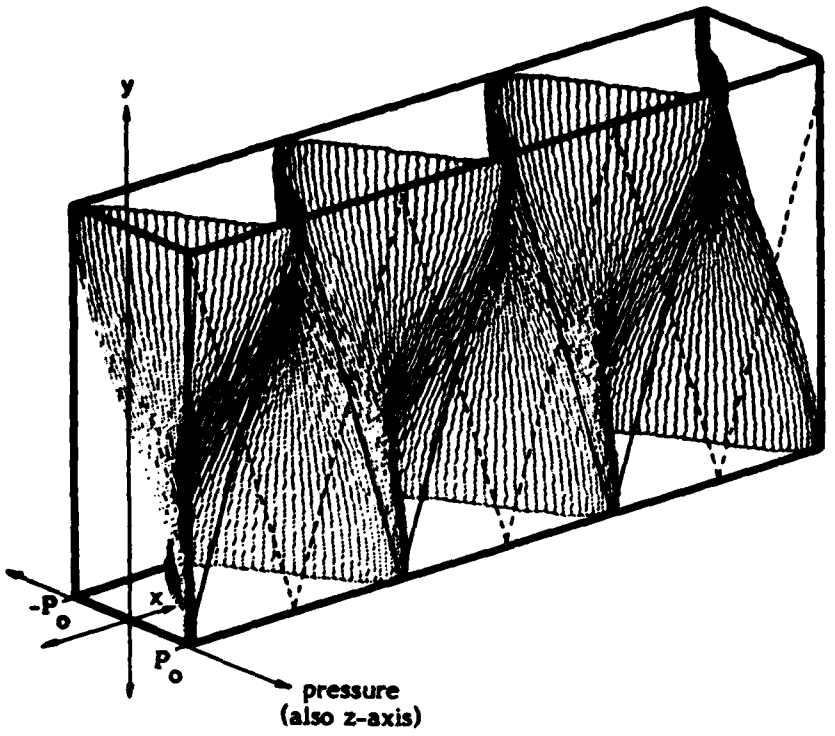

(a) Instantaneous pressure field

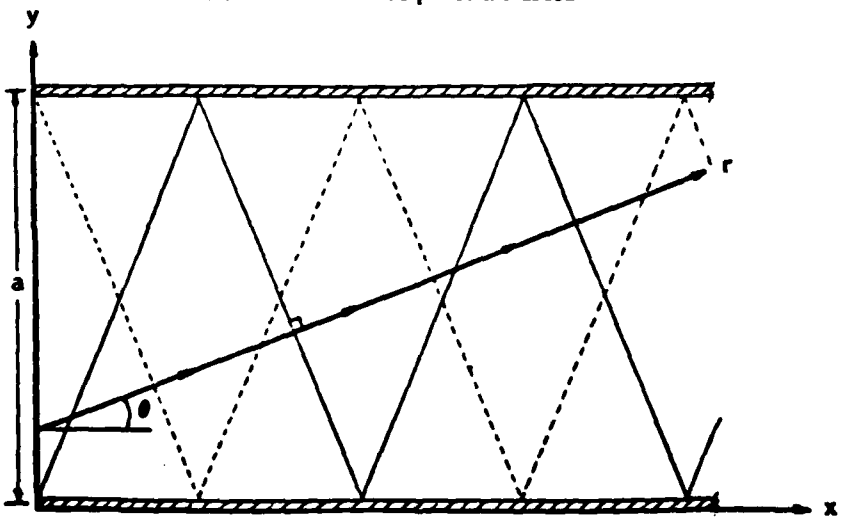

(b) Projection showing propagation direction of the (1,0) mode

Figure 2.5

Pressure field of the (1,0) mode

ARL:UT
AS-84-587
JATC - GA
7 - 9 - 84

The periodicity relation (see Eqs. (2.25) and (2.28)) becomes

$$\Delta x = \frac{2\pi \cos\theta}{k_p(1 - \cos\theta)} \quad . \tag{2.33}$$

E. Tube wall attenuation and dispersion

Since the interaction between the two modes occurs in a waveguide, the theory presented must be modified to include tube wall effects if predictions of the theory are to be compared with experimental results. The most prominent tube wall effect is attenuation. Attenuation of the (0,0) mode as well as the (1,0) mode must be considered. Another tube wall effect, dispersion, is briefly considered at the end of this section.

For the range of frequencies we consider here losses within a tube are mainly due to boundary layer effects. The viscous boundary layer (vbl) has a thickness,[40]

$$Y_{vbl} = \sqrt{\frac{2\nu}{\omega}} \quad ,$$

where ν is the kinematic viscosity of the fluid. The thickness of the thermal boundary layer (tbl) is

$$Y_{tbl} = \frac{Y_{vbl}}{\sqrt{Pr}} \quad ,$$

where $Pr = C_p\eta/\kappa$ is the Prandtl number, C_p is the specific heat at constant pressure, η is the shear viscosity coefficient, and κ is the heat conduction coefficient. Since $Pr \cong 0.7$ for air, the two boundary layers have about the same thickness. Moreover, for most frequencies the boundary layers are remarkably thin.

At 500 Hz, for example, $Y_{vbl} < 0.1$ mm. When the boundary layer thickness is small compared to the tube cross section,* the following expression holds:

$$\alpha_o = \frac{1 + (\gamma - 1)/\sqrt{Pr}}{Dc_o} \sqrt{2\nu\omega} \quad , \tag{2.34}$$

where α_o is the plane wave or (0,0) mode attenuation coefficient and D is the hydraulic diameter of the tube.†

Attenuation of modes other than the (0,0) is also of importance in our study. Hartig and Lambert[43](1949) attempted to predict the attenuation of the (1,0) mode in a waveguide by modifying Eq. (2.34) so that it includes the extra travel distance of the mode. This modification, however, proved to be inadequate. A later analysis by Bogert[44](1950), while more complete than Hartig and Lambert's, failed to properly include thermal losses. Finally, both Beatty[45](1950) and Shaw[46](1950) independently reported complete theories to describe the attenuation. Moreover, these authors developed expressions for the attenuation of any (m,n) mode. Beatty used expressions for attenuation (developed by Morse[47]) which apply for rectangular ducts with uniform, small wall admittances. He then extended the expressions to apply to ducts with different side wall admittances. Combining Morse's formulae with an expression for boundary layer admittance as a function of the angle of incidence, the author developed an expression for the attenuation of any mode. It is interesting to note that the viscous boundary layer losses vary as $\cos^2\theta$ whereas the

*The waveguide used in our experiments fits the definition of a "wide tube" for the frequencies we consider.[41] A wide tube is one in which the boundary layer does not occupy a large portion of the volume in the tube. Conversely, the tube may not be so large that the mainstream effects are more prominent than those of the boundary layer. Further discussion may be found in Pestorius.[42]

†For a waveguide of cross-sectional dimensions $a \times b$, $D = 2ab/(a+b)$.

thermal boundary layer losses do not depend on angle. The difference arises because of the same vector-scalar considerations made to determine the form of β_{eff}. Beatty's result for the attenuation coefficient of the (1,0) mode (α_1) is

$$\frac{\alpha_1}{\alpha_o} = \frac{1}{\sqrt{1-\left(\frac{f_c}{f}\right)^2}}\left[\frac{R+2}{R+1} - \left(\frac{f_c}{f}\right)^2 \frac{2}{(R+1)(W+1)}\right] , \qquad (2.35)$$

where R is the ratio of the long dimension to the short dimension of the cross section and $W = (\gamma - 1)/\sqrt{Pr}$. Actually, Eq. (2.35) is valid for any (m,0) mode. The equation has the order of the mode already built in. One merely needs to choose the appropriate value of f_c for the particular mode of interest. With the proper modal attenuation coefficients in hand, we may proceed to modify the interaction theory to include the effect of losses.

The expression for the modulation index, Eq. (2.23), involves only the amplitude of the pump. The attenuation of the weak wave is therefore ignored for the moment. Schaffer's treatment[29] of the attenuation is applicable here. For a slowly varying pump amplitude, the modulating effect of the pump over a given distance is determined by the average amplitude over that distance. Schaffer thus defines an average Mach number $\bar{\epsilon}_p$ as follows:

$$\bar{\epsilon}_p = \frac{1}{x}\int_0^x \epsilon_p e^{-\alpha_o x'}\, dx' = \epsilon_p \frac{1 - e^{-\alpha_o x}}{\alpha_o x} . \qquad (2.36)$$

Substitution of $\bar{\epsilon}_p$ for ϵ_p throughout the analysis serves as the basis for accounting for attenuation in all of our measurements.*

*If we use the substitution $\epsilon_p \exp(-\alpha_o x)$ for ϵ_p, we obtain what Schaffer calls a "full attenuation" theory. The use of this substitution, however, overcompensates for the attenuation effect.

Although the attenuation of the (1,0) mode is not considered in the preceding analysis, its value is more than academic. The effects of attenuation of the (1,0) mode are important when we examine the effects of geometric dispersion. Equation (2.24) and Eq. (2.27), which represent the amplitudes of the primary and sum and difference frequency wave components, both need to be modified to include attenuation. By replacing u_{ow} with $u_{ow}e^{-\alpha_1 x}$ we obtain the following modified equations:

$$\left|\frac{u_{wc}}{u_{ow}}\right| = \left| e^{-\alpha_1 x} J_0\left(\mu \frac{\sin\Psi}{\Psi}\right)\right| \tag{2.37}$$

and

$$\left|\frac{u_{\pm}}{u_{ow}}\right| = \left| e^{-\alpha_1 x} J_1\left(\mu \frac{\sin\Psi}{\Psi}\right)\right|. \tag{2.38}$$

The behavior of the components is now different from that shown in Fig. 2.3. The expected behavior--with attenuation--is shown in Fig. 2.6.

Finally, the effects of tube wall dispersion should be mentioned. The frequency dependent sound speed in a tube is[41]

$$c(\omega) = \frac{c_o}{1 + c_o\alpha_o/\omega} .$$

For the frequencies used in this study the difference between $c(\omega)$ and c_o is extremely small. At 4 kHz, for example, there is less than 0.2% difference between $c(\omega)$ and c_o. The effects of tube wall dispersion may therefore be safely ignored.

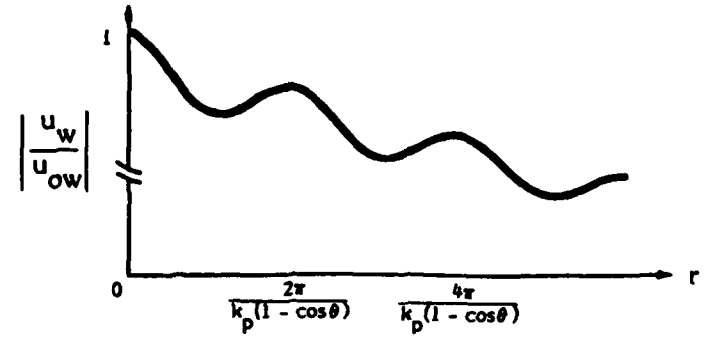

(a) Amplitude of component at frequency f_w

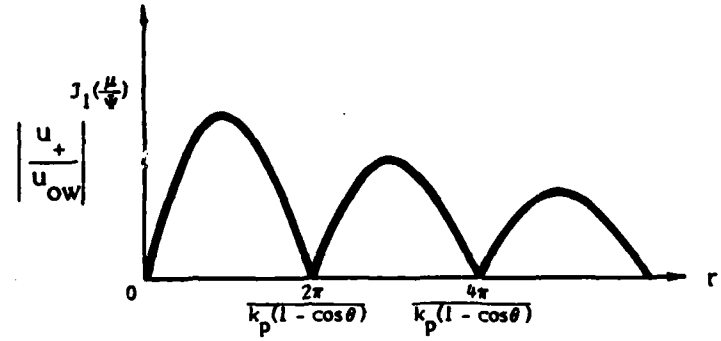

(b) Amplitude of component at sum frequency

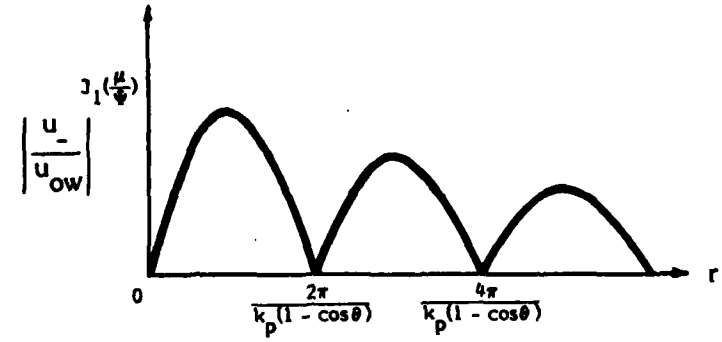

(c) Amplitude of component at difference frequency

Figure 2.6

The effect of geometric dispersion
and tube wall attenuation

CHAPTER 3

EXPERIMENTAL APPARATUS AND PRELIMINARY TESTING

This chapter contains a description of the experimental apparatus and an account of preliminary measurements used to test it. Discussion of the apparatus section is divided into three parts. First the waveguide is described, then the transmit system, and finally the receive system. The second half of the chapter is devoted to measurements of the waveguide's anechoic termination, (1,0) mode behavior, and tube wall attenuation.

A. Apparatus and design

Described in this section are the waveguide, the acoustic drivers and their interface with the waveguide, and the receive system (microphones and related equipment). An overall block diagram of the waveguide and the apparatus is shown in Fig. 3.1.

1. Waveguide

A rectangular waveguide was used. A sketch of the waveguide and its support systems is shown in Fig. 3.1(a). Many things were considered before a specific waveguide was selected. The throat of the compression driver used for producing the finite-amplitude wave is 50 mm in diameter. We chose the cross-sectional area of the waveguide to be as close to that of the driver's throat as possible. It was hoped that this choice would eliminate the need for a circular-to-rectangular transition section to join the driver to the waveguide.* Another consideration was the difference between the cut-on frequencies of the (1,0) mode

*This hope was in fact realized although some steps were taken to make the transition less abrupt; see Section 2 of this chapter.

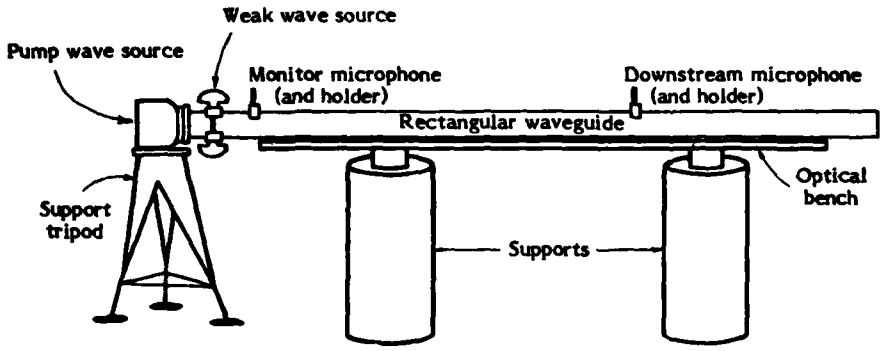

(a) Waveguide and associated equipment

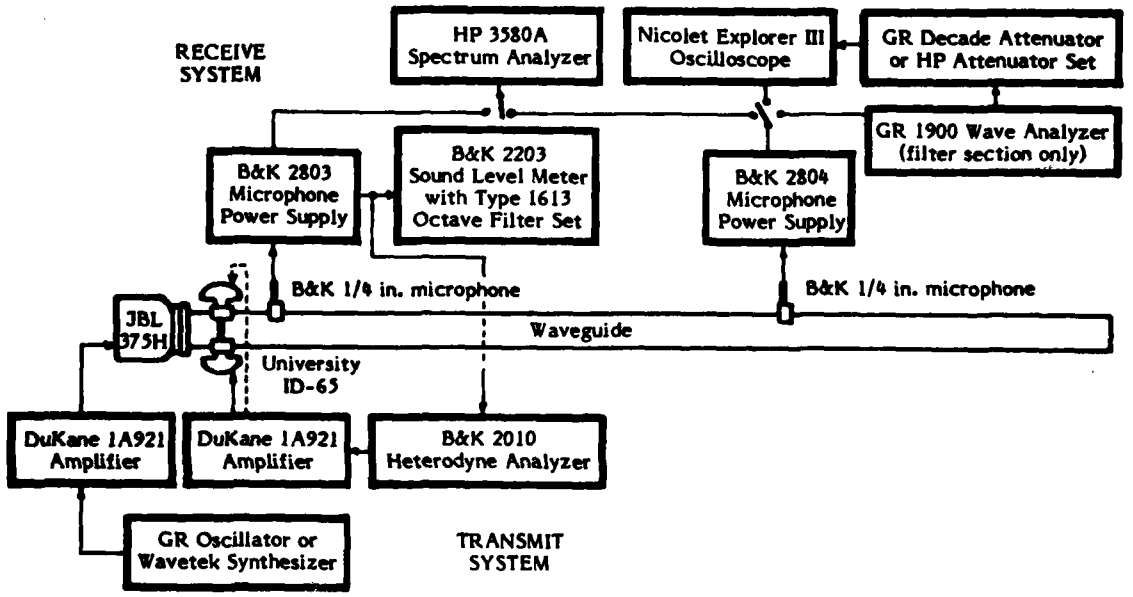

(b) Block diagram of measurement apparatus

Figure 3.1

Experimental apparatus

ARL:UT
AS-84-589
JATC - GA
7 - 9 - 84

and the next higher mode. The waveguide cross-sectional dimensions should be such that a large range of intersection angles between the (0,0) and (1,0) modes is obtainable before the next mode intrudes. A waveguide with a perfectly square cross-section, for example, is unsuitable because both the (1,0) and (0,1) modes have the same cut-on frequency. The ideal ratio of the two cross-sectional dimensions is, in fact, 2 to 1 (see Eq. (2.30)). The size of the drivers with which we planned to excite the (1,0) mode was another consideration. Finally we chose the length of the waveguide. The waveguide should be as long a single unit as possible; multiple waveguide sections may have discontinuities.

The waveguide selected for the experiments was locally obtained: a 6.4 m (21 ft) section of aluminum ducting with inside cross-sectional dimensions (a × b) of 70 mm × 38 mm (2.75 in. × 1.5 in.) and 3.2 mm (1/8 in.) thick walls. The first several cut-on frequencies for this waveguide are listed in Table 3.1.

Table 3.1

Mode cut-on frequencies
(c_o = 343 m/sec)

Mode (m,n)	f (Hz)
1,0	2465
0,1	4540
2,0	4930
1,1	5165
2,1	6700
3,0	7390

The range in angles of intersection between the (1,0) and (0,0) modes before the next highest mode might intrude may be easily calculated from Eq. (2.31) and Table 3.1. At the cut-on frequency of the (1,0) mode, 2465 Hz, the angle of intersection

between the (1,0) mode and the principal mode is 90°. At the cut-on frequency of the (0,1) mode, 4540 Hz, the angle of intersection is 33°.

Since the waveguide had to be accessible along its full length, its mounting was important. After the ends of the waveguide were machined square, the waveguide was placed on a long optical bench which was securely mounted to the laboratory floor. Rubber mats between the waveguide and the bench provided vibration isolation. The waveguide was oriented on the optical bench with the a dimension vertical (see Fig. 2.4). In this way, the microphones utilized to measure the (1,0) mode could be conveniently positioned on the top of the waveguide.

Microphone holes, or ports, were drilled through the walls of the waveguide. All but one of the ports were located along the centerline of the top wall. Both the (0,0) and (1,0) modes could be measured from these ports but not the next higher, and undesirable, (0,1) mode. For detection of the (0,1) mode, a single hole was drilled in one of the side walls. A diameter of 9.80 mm (0.386 in.) was chosen for all ports in order to match the size of various ⅜ in. teflon microphone holders which had been previously machined for another progressive wave tube. The first port was located a short distance (125 mm) from the source end in order to accommodate the two side-mounted drivers. The spacing scheme for the ports is given in Table 3.2. Note that the sidewall port is No. 16, 3.1 m from the reference port. No microphone holes are listed beyond 5.1 m because an anechoic termination occupied this space. When not in use, each port was stopped with an aluminum plug machined to fit flush with the inside wall of the waveguide. Duct seal was used on the outside to make an acoustically tight fitting.

Table 3.2

Microphone port spacing

Hole #	Position (m)	Hole #	Position (m)
1	reference (0.0)		
2	0.1	14	2.7
3	0.2	15	3.0
4	0.4	16 (side port)	3.1
5	0.6	17	3.3
6	0.9	18	3.6
7	1.2	19	3.9
8	1.3	20	4.2
9	1.5	21	4.3
10	1.8	22	4.5
11	2.1	23	4.8
12	2.3	24	5.0
13	2.4	25	5.1

To allow only progressive traveling waves in the waveguide, we constructed an anechoic termination 1.2 m long having a full wave tangent taper (see Burns[48]). The termination was designed to have a reflection coefficient $|R| \leq 0.01$ (level of the reflected wave at least 40 dB below the level of the incident wave) for frequencies above 400 Hz. The first 0.7 m consisted of ordinary fiberglass cut with a tangent taper. The remaining 0.5 m consisted of alternately packed fiberglass and batted Kevlar®29 Aramid.* Alternating the packing was found empirically to enhance the absorption for frequencies in the range 500 Hz to 900 Hz. Tests performed on the termination are discussed in a later section of this chapter.

*Manufactured by duPont de Nemours & Co., Wilmington, Delaware.

2. Transmit system

The various items of equipment used to produce the two waves in the waveguide are listed below.

JBL-375 H Compression Horn Driver (aluminum diaphragm)

JBL-375 H Driver with D16R2441 aluminum diaphragm

JBL-375 H Driver with D16R2482 phenolic diaphragm

University Sound ID-65 Horn Driver (2)

Wavetek Model 171 Synthesizer/Function Generator

General Radio (GR) Type 1310-A Oscillator

GR Type 1396B Tone-Burst Generator

B&K Type 2010 Heterodyne Analyzer
(beat frequency oscillator section)

DuKane Type 1A921 200 W Power Amplifier (2)

The interface between several of these items and the waveguide is now discussed.

How to excite the (1,0) mode was an important problem in the design of the entire transmit system and thus is discussed first. Ideally, one might fit a split rectangular piston to the end of the waveguide. If half of the piston could be driven 180° out of phase with respect to the other half, one would have an ideal source for generating of the (1,0) mode. Unfortunately, such a piston is difficult to construct. A source which nearly reproduces the excitation of the ideal, split piston was used by Hartig and Lambert[43] in their study of (1,0) mode attenuation in waveguides. They used a plate with two holes in it. Each hole, which was made as large as possible, was connected to a telephone receiver. The receivers, acting as sources, were connected 180° out of phase (reversed leads) to a single oscillator. Together, the two receivers formed the source. Shaw[46] used a similar but slightly improved

method: he added a way to change the phase and amplitude of one of the sources. His observations led him to conclude that small differences in the phase and amplitude of the two sources made little difference in the excitation of the mode. Ghabrial[49] devised yet another variation on the two-hole scheme. His source was a standing wave tube. The tube was designed and placed so that the two holes, which connected the tube to the end of the waveguide, were positioned at successive pressure nodes of the standing wave. Because the particle velocities at the two nodes are perfectly out of phase, the (1,0) mode was easily excited. None of these methods, however, were well-suited for our investigation. We needed to excite the (0,0) mode as well as the (1,0) mode.

Our source configuration design is simple. If the (1,0) mode source is placed in the walls of the waveguide, the principal mode source may be mounted in the end. The sound field produced by pistons flush-mounted in the walls has, in fact, even been analyzed.[50] Details of our design now follow.

Various driver and diaphragm combinations were used to generate the principal mode. As noted in Section 1, range of frequencies available for the (1,0) mode is about 2500 Hz to about 4600 Hz. Since the condition $\omega_w >> \omega_p$ must hold if the theory is to be appropriate, a very low frequency source was necessary to generate the (0,0) mode. We selected a JBL-375 H compression horn driver. Although several units had been obtained for earlier studies, all eventually failed. Two types of diaphragms were obtained to repair the units.* An aluminum JBL-D16R2441 diaphragm was used first. Its major advantage is its wide frequency response, 500 Hz to 16 kHz ($\pm$5 dB). In its design housing (the JBL 2441 compression

*Diaphragms originally designed for the JBL-375 H are no longer available.

driver) this diaphragm is rated to handle approximately 50 W rms (continuous sine). However, in the JBL-375 H housing, the diaphragm could withstand only 25 W rms (approximately) at 500 Hz. Above this level the diaphragm usually separated from its mounting ring. Several diaphragms were lost this way. Although the cause may have been mounting and fitting misadjustment in the JBL-375 H housings the actual cause remains unknown. Another difficulty with the modified drivers, especially at low frequencies and high input powers, was distortion. At 20 W rms input at 500 Hz the second harmonic sound was typically only 10 dB below the fundamental sound. Another JBL-375 H housing fitted with a JBL-D16R2482 phenolic diaphragm was also used. Although the frequency response of the phenolic diaphragm unit was limited to the range 300 Hz to 5 kHz, distortion was not a problem: the second harmonic was greater than 20 dB below the fundamental in all cases. A slight limitation of this unit was the limited excursion of the diaphragm within the confines of the driver housing. At extremely high input levels and low frequencies (e.g., 400 Hz) the diaphragm actually contacted the phase plug (the contact was identified by a pronounced, angry buzzing sound). Although no damage to the diaphragm was observed, the conditions causing the contact were thereafter avoided.

Two connecting flanges were used to couple the JBL-375 driver to the waveguide. The flanges are shown in Fig. 3.2 (the coin next to the driver is shown for scale). Duct seal, not shown in the photograph, was used as a filler on the inside between the two flanges to make the circular-to-rectangular shape change less abrupt. The duct seal also served as an acoustical seal.

The method used to excite the (1,0) mode is quite simple. The arrangement we chose is shown in Fig. 3.3. A pair of slots, 3.1 mm 30 mm, were cut in

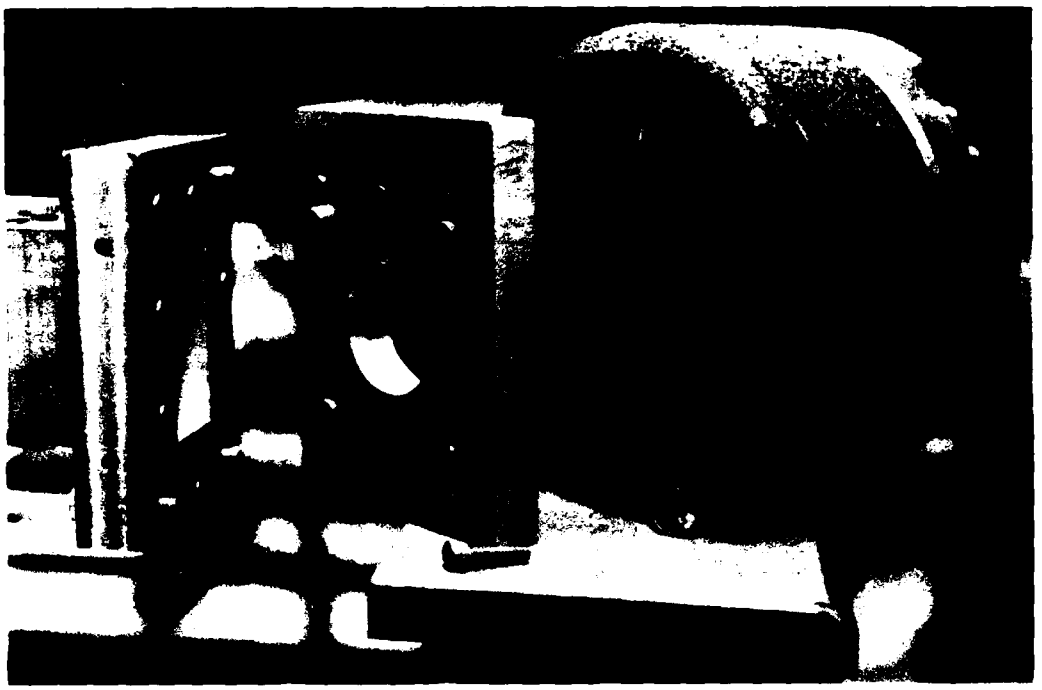

Figure 3.2

Connection between
JBL-375 driver and waveguide

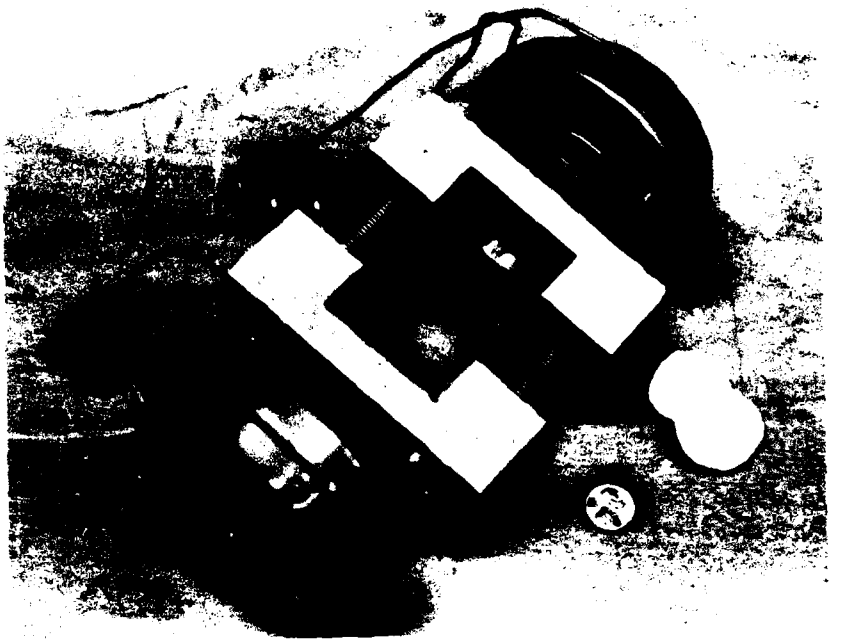

(a) ID-65 drivers and mounting blocks

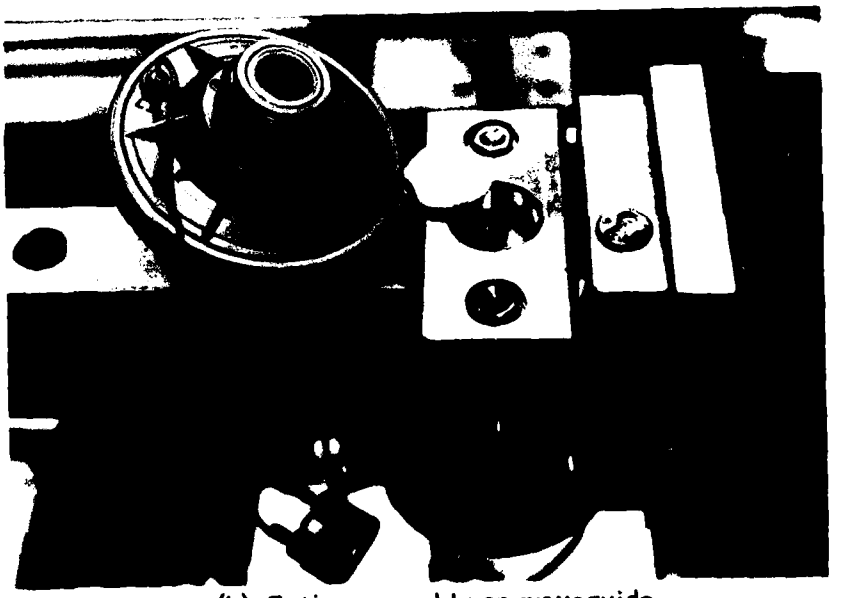

(b) Entire assembly on waveguide
(top driver removed to show slot port)

Figure 3.3

Connection between
ID-65 drivers and waveguide

the waveguide, one across the top and one across the bottom. Slots were chosen rather than holes because we wished to excite the (1,0) mode across the entire b dimension of the cross-section. Each slot served as a port for a University ID-65 driver. Two aluminum mounting blocks, each threaded to accept one of the drivers, were fit over the slots. Figure 3.3(a) shows the two drivers and their mounting blocks. Fig. 3.3(b) shows the system (with one of the drivers removed to reveal the slot) together with the connecting flanges; to the right are the JBL-375 H driver and its mount to the waveguide. Acoustic coupling between the JBL-375 H and the University drivers was found to be troublesome. In particular, increasing the sound from the JBL-375 H caused a decrease in the sound from the ID-65 drivers. The coupling was reduced by fitting two 5 mm thick disks of needled and felted Kevlar®29 (shown in both photos although not in place) to the inside of the mounting blocks, i.e., between the slots and the drivers. The Kevlar®29 acted as a buffer to isolate the ID-65 drivers from the intense low frequency sound. The small lump to the left of the ID-65 driver is a microphone port plug covered with duct seal. Figure 3.4 shows all three drivers completely assembled (the plug for the reference microphone port has been removed and is visible to the left of the ID-65 driver).

Various oscillators and amplifiers were used with the drivers to generate the two waves. These make up the rest of the transmit system and may be found in the lower portion of Fig. 3.1(b). After the two University ID-65 drivers were mounted to the waveguide, they were electrically connected in parallel but 180° out of phase (i.e., reversed leads)* to one of the DuKane amplifiers, which was fed by an oscillator or synthesizer. Our attempts to improve the (1,0) mode excitation by

*At times the two drivers were connected in phase in order to generate a high frequency signal in the (0,0) mode.

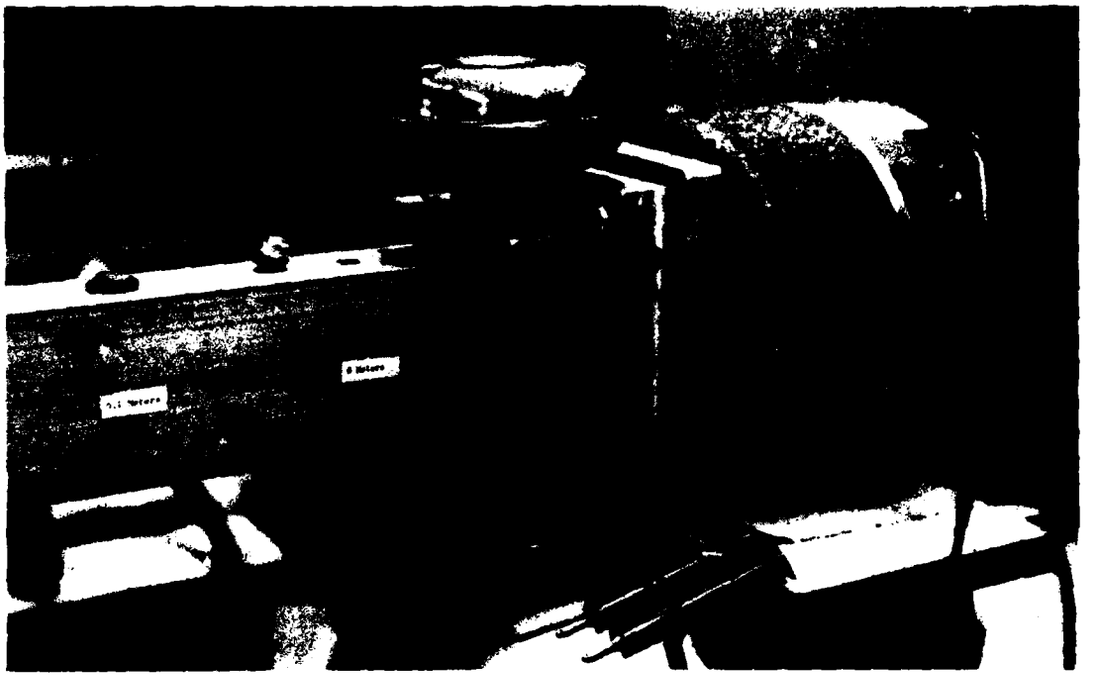

Figure 3.4
Complete assembly of sources

adjusting the amplitude and phase of one of the drivers produced no significant results. Whenever it was important to maintain a constant source level from these two drivers, they were connected to the beat frequency oscillator of the B&K 2010 heterodyne analyzer and a DuKane amplifier. The B&K 2010 has a compressor circuit, or automatic gain control (AGC), which, used in conjunction with a microphone at the reference port, made it possible to maintain a sound pressure level constant to within $\pm$0.2 dB. The electrical power for the JBL-375 H driver was provided by another DuKane amplifier, which followed the Wavetek synthesizer or a sine wave generator. An investigation of the performance of the transmit system is given later in this chapter.

3. Receive system

The following components made up the receive system:

Hewlett-Packard (HP) 3580A Spectrum Analyzer

Nicolet 2096 Explorer III Digital Oscilloscope

B&K Type 2203 Precision Sound Level Meter

B&K Type 1613 Octave Filter Set

GR 1900 Wave Analyzer (filter and amplifier sections)

GR Type 1450-TB Decade Attenuator

HP 350C Attenuator Set

HP 5216A 12.5 MHz Electronic Counter

B&K Type 2010 Heterodyne Analyzer

B&K Type 2604 Microphone Amplifier

B&K Type 2803 Two Channel Power Supply

B&K Type 2804 Microphone Power Supply (2)

B&K Type 4136 ¼ in. Condenser Microphone (2)

B&K Type 4134 ½ in. Condenser Microphone

B&K Probe Tube Set UA 0040

B&K Type 4220 Pistonphone (2)

B&K Type 2619 Microphone Preamplifier (3)

HP 3575A Gain/Phase Meter

A block diagram showing the arrangement of the most important of these items may be found in the upper portion of Fig. 3.1(b).

The microphones listed above were a vital part of the experiments. Each was used for a distinct measurement. One ¼ in. microphone was used exclusively as the monitor (at the reference port). The other ¼ in. microphone was mounted in one of the top wall ports to measure the sound field downstream. Each ¼ in. microphone fit inside a specially machined teflon holder (see Fig. 3.5(a)). This holder, in turn, fit inside a machined nylon block, which straddled the top of the waveguide. The entire assembly, shown in Fig. 3.5(b), was held in place with two elastic bands. Mounted in this fashion, the microphone face was flush with the inside wall of the waveguide. The ½ in. microphone was fit with a 2 mm diam, 100 mm long probe and used to measure the field across the waveguide (from side to side or top to bottom). The tube of the probe microphone fit snugly in a hole drilled in a nylon plug, which in turn fit in one of the ports. Figure 3.6 shows the probe tube inserted about halfway into the waveguide.

The microphone outputs were processed or measured with the following equipment. The filter and microphone amplifier sections of the GR 1900 wave analyzer were often used with either the downstream microphone or the probe tube microphone. The analyzer's narrow passband filter (10 Hz) was ideal for examining the primary component of the modulated weak wave, especially in the presence of

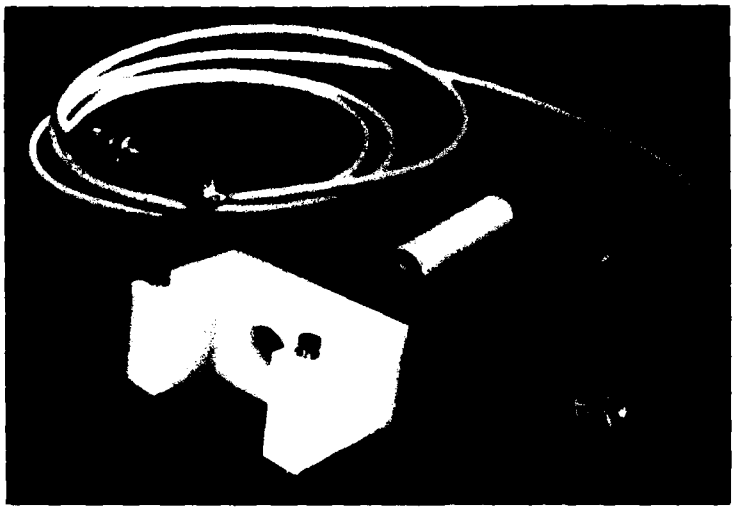

(a) Disassembled downstream microphone assembly

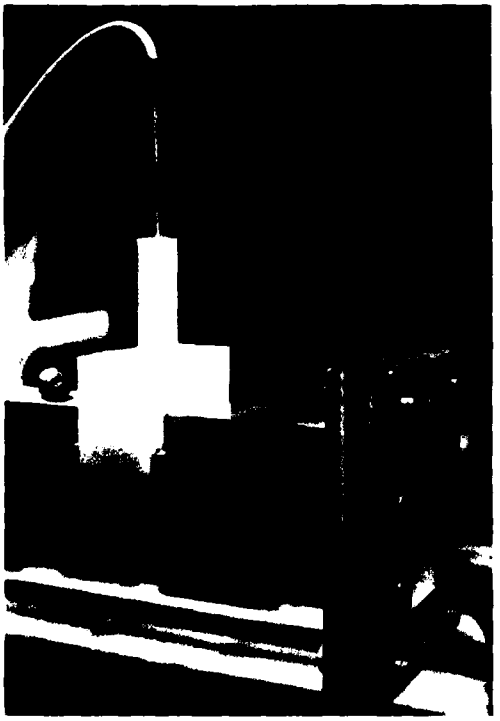

(b) Monitor microphone assembly attached to waveguide

Figure 3.5
Microphone assemblies

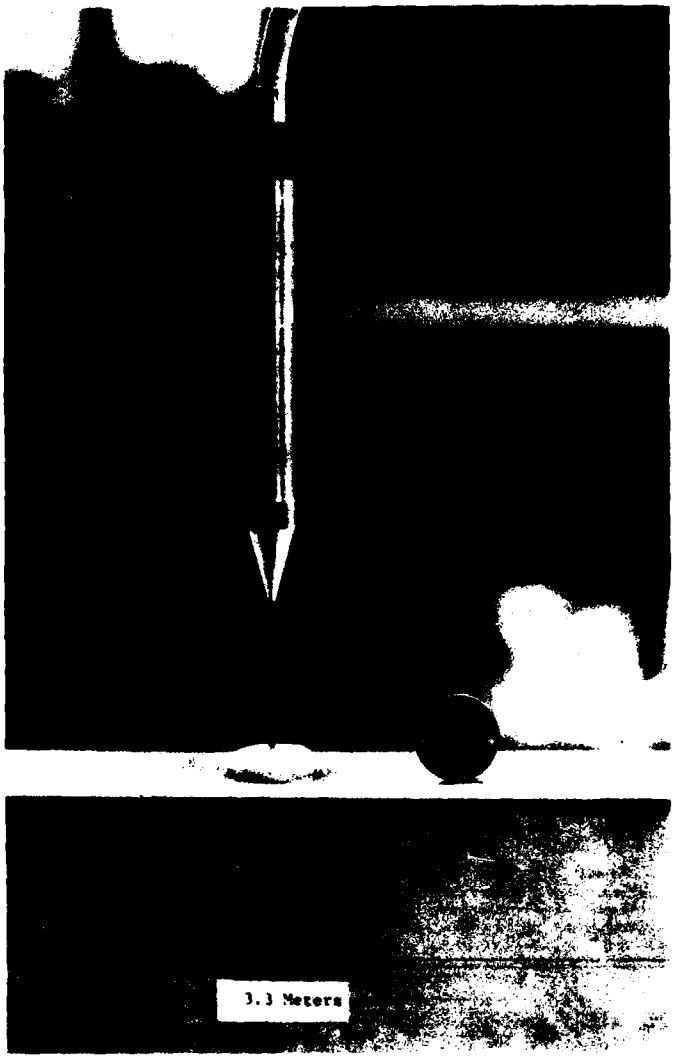

Figure 3.6

Probe tube microphone assembly

the strong pump signal. The storage capablities of the Nicolet Digital Oscilloscope were frequently used to manipulate and measure waveforms obtained at the downstream microphone position. The HP 3580A spectrum analyzer was used alternately with the downstream and monitor microphones. To measure the pump wave level, a B&K 2203 sound level meter with a 1613 octave filter set was used. The characteristics of the filter set were carefully checked to ensure accurate readings.

All of the microphones and analyzers were calibrated with a B&K 4220 pistonphone before each set of experiments was run. This pistonphone was itself compared with another identical and recently calibrated* B&K pistonphone borrowed from a local firm. The outputs of the two pistonphones agreed within $\pm$0.2 dB.

B. Equipment tests and determination of waveguide properties

1. Anechoic termination

The function of the anechoic termination was to prevent reflections from the end of the waveguide. It had to be effective for both the (0,0) and (1,0) modes and therefore work over a wide range of frequencies. For the range 400 Hz to 2 kHz, the performance of the termination was tested by using tone bursts. For these tests, the two ID-65 drivers were removed and the two slots covered with duct seal. The Wavetek synthesizer, the GR tone-burst generator, and a JBL driver were were used to generate four to six cycles at each frequency. A ¼ in. microphone was positioned so that both the incident and reflected tone bursts could be captured and resolved on the Nicolet oscilloscope. The level of the reflected wave relative to that of the incident wave is given as a function of frequency in Fig. 3.7. Although

*It had been calibrated 4 months prior to these experiments.

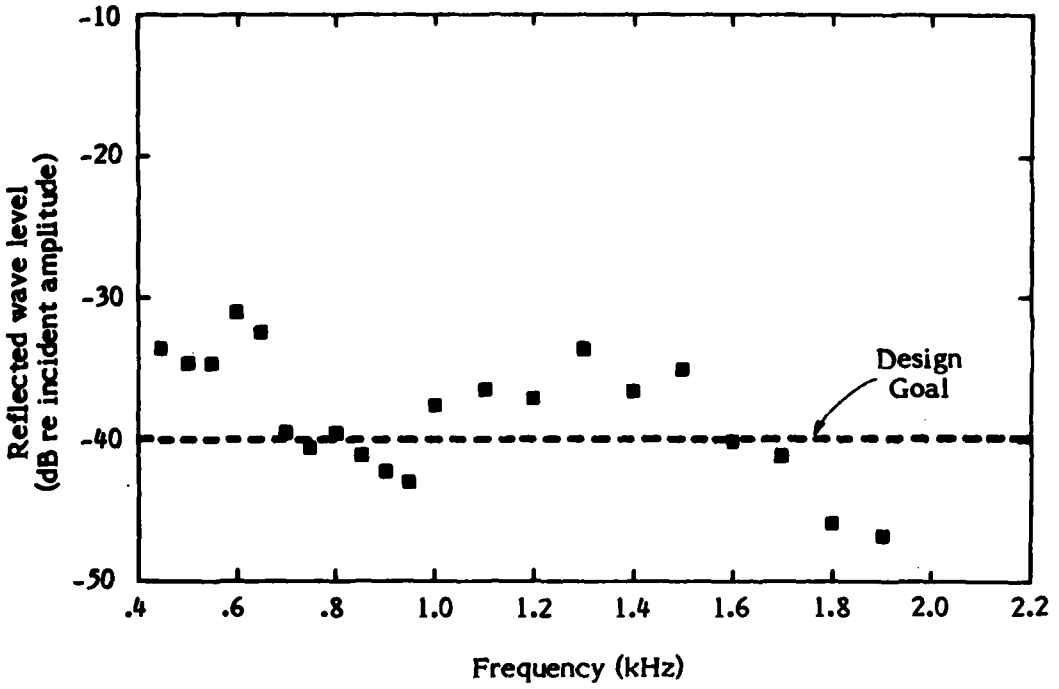

Figure 3.7

Reflection coefficient for anechoic termination as a function of frequency

ARL:UT
AS-84-590
JATC - GA
7 - 9 - 84

the design goal was not met at all frequencies in the range shown in the figure, the reflection was never large enough to be troublesome.

The dispersive properties of the waveguide became quite apparent when we tried to use the tone burst method to test the termination above 2 kHz. The initial, clearly defined tone burst, which is wideband in nature, became a pulse with

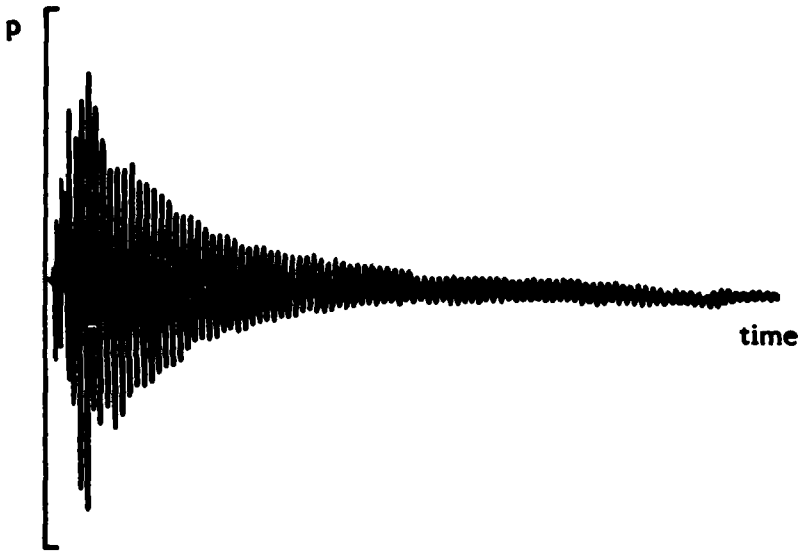

Figure 3.8
Typical pulse wake

ARL:UT
AS-84-591
JATC - GA
7 - 9 - 84

a wake.† A pulse captured during a tone burst experiment is shown in Fig. 3.8. The presence of wakes makes it nearly impossible to use short tone bursts to evaluate

†See, for example, Morse and Ingard,[39] pp. 498 ff. The components of the pulse whose frequencies are higher than the (1,0) mode cut-on frequency may travel in either the (0,0) or (1,0) mode. Those components traveling in the (1,0) mode have travel speeds which depend on their frequencies.

the termination. An attempt to use very long tone bursts, which have less significant wakes, did not yield any measurable results. No reflected pulses could be detected. Similar results were obtained using long tone bursts of the (1,0) mode. Thus, although it was not possible to measure the reflection above 2 kHz, the qualitative tests with the tone bursts, combined with the trend shown in Fig. 3.7, made it quite certain that the higher frequency waves were effectively absorbed by the termination.

2. (1,0) mode behavior

The performance of the sources used to produce the weak wave is now discussed. How effective was our method of generating the (1,0) mode? To measure the weak wave field within the waveguide, we employed the probe tube microphone (inserted through one of the top ports), the GR wave analyzer and the Nicolet oscilloscope. A probe into the waveguide at the 2.7 m port revealed pressure antinodes at both top and bottom walls and a node at the center. Use of the HP gain/phase meter showed that the pressures at the two walls were 180° out of phase. Plots of the pressure field obtained at 2700 Hz and 4300 Hz are presented in Fig. 3.9. For our experiments the frequency of the weak wave was below the cut-off frequency of all but the (0,0) and (1,0) modes. The (0,0) mode is, unfortunately, easy to excite. The depth of the pressure node was therefore an excellent indication of the composition of the wave field. A deep null implies that the field is mainly composed of the (1,0) mode. A shallow minimum, on the other hand, indicates the presence of the principal mode as well. Node pressure was 20 dB to 30 dB down from the wall pressure for the noncollinear experiments in the following chapter.

If the (1,0) mode source frequencies are kept below 5 kHz, only one unwanted mode, the (0,1), may be excited, and it only in the region above about

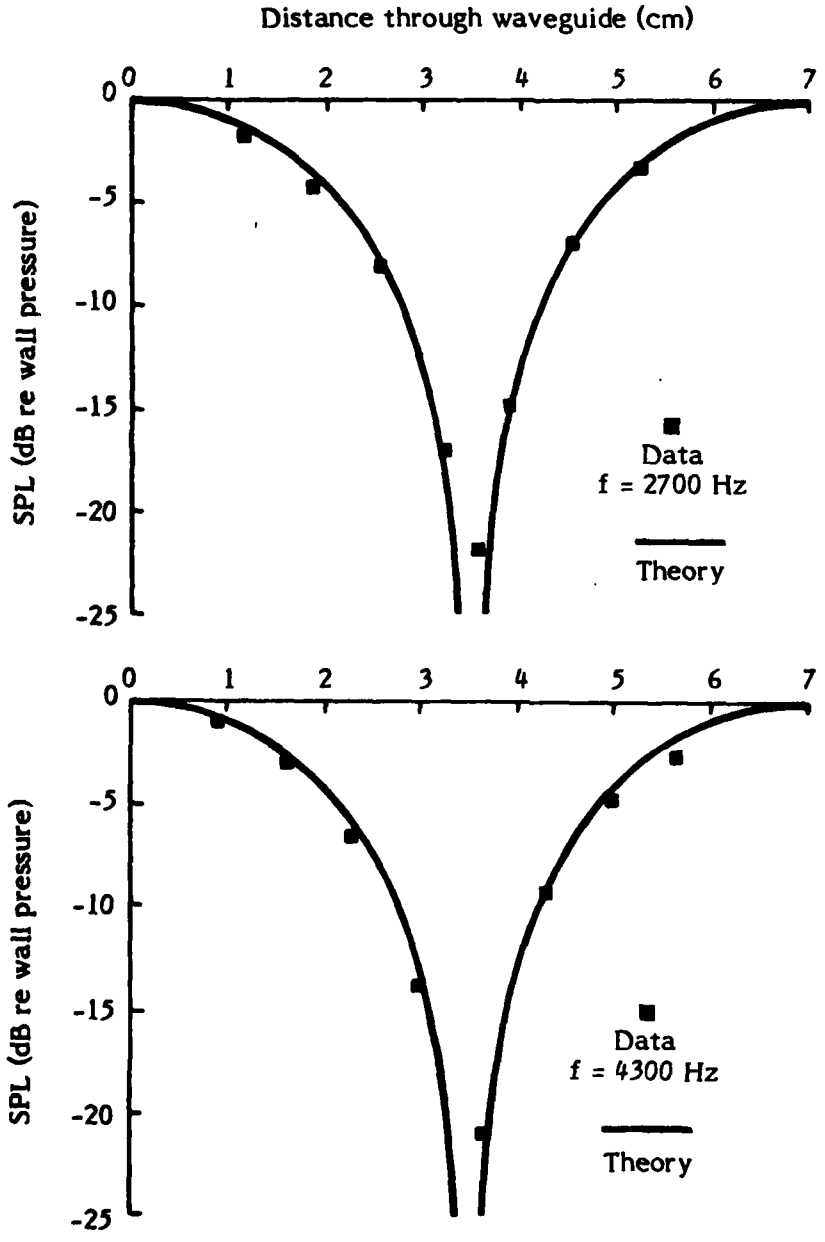

Figure 3.9

Probe tube scan through waveguide showing the presence of (1,0) mode

ARL:UT
AS-84-592
JATC-GA
7-9-84

4.5 kHz. The extent to which this mode affects measurements is another question which arises. Our observations were as follows. Generally, the (0,1) mode appeared only when the source frequency was at, or immediately above, its cut-on frequency. This behavior occurred regardless of the source configuration used. As source frequencies got higher, the (0,1) mode vanished. Source conditions were not favorable for its existence.*

The waveguide's response near the cut-on frequency of any given mode is quite interesting. As long as the source frequency is below the cut-on frequency of the mode, the SPL in the waveguide remains fairly constant. At the mode's cut-on frequency, however, the SPL rises rapidly. The behavior described occurs regardless of the source used. The abrupt increase is easily explained. At cut-on frequency the mode is nearly a standing wave. Very little energy is necessary to excite and maintain it. Maintaining a particular mode above its cut-on frequency, however, depended strongly on the source configuration chosen. As noted above, the (0,1) mode died quickly as the source frequency rose above its cut-on frequency. Without the out-of-phase ID-65 drivers as sources, the (1,0) mode vanished as well.*

3. Tube-wall attenuation

a. Principal mode

Tone bursts were used to measure the attenuation coefficient of the principal mode in the waveguide. Two microphones and the Nicolet oscilloscope were utilized. The first microphone was employed to measure an initial tone burst generated by a JBL driver; the other microphone, positioned much farther downstream, measured the attenuated tone burst. Both tone bursts were captured and stored in the memory of the Nicolet oscilloscope. After the different

*See Doak[50] for a thorough analysis of excitation and transmission of sound in rectangular waveguides.

sensitivities of the two microphones had been taken into account and the distance between the two microphones recorded, the plane wave attenuation coefficient at the tone burst frequency was calculated. This process was repeated with several different microphone separations. The average attenuation coefficient as a function of frequency is presented in Fig. 3.10. The functional relationship between the attenuation coefficient and frequency is found by a least squares fit to the data: the result is $\alpha(\text{Np/m}) = (1.10 \times 10^{-3})\, f^{0.517}$. Although the results compare favorably with the predictions of Kirchhoff attenuation theory, Eq. (2.34), the plot shows that the data tend to be roughly 3% higher than predicted by the theory--this tendency is comparable to similar trends noted by other authors.* As was the case in testing the anechoic termination, dispersion inhibited any further measurements at frequencies higher than 2 kHz. At these frequencies, however, it is the attenuation of the (1,0) mode, not the (0,0) mode, in which we are most interested.

b. (1,0) mode

The value of the attenuation coefficient as a function of frequency for the (1,0) mode was determined using a continuous wave and a single microphone. The (1,0) mode was generated by the two ID-65 drivers. For each frequency, the SPL was measured as a function of distance. The attenuation coefficient as a function of frequency is shown in Fig. 3.11. These data are plotted along with the theoretical prediction of Beatty[45] and Shaw.[46] The attenuation coefficients have been normalized with respect to the theoretical Kirchhoff plane wave attenuation coefficients (α_o). Note that the data extend to roughly 5000 Hz. Beyond this frequency other modes appeared and measurements became extremely difficult. In general, the data presented in Fig. 3.11 agree remarkably well with the theory presented by both Beatty and Shaw.

*See, for example, Mariens.[51]

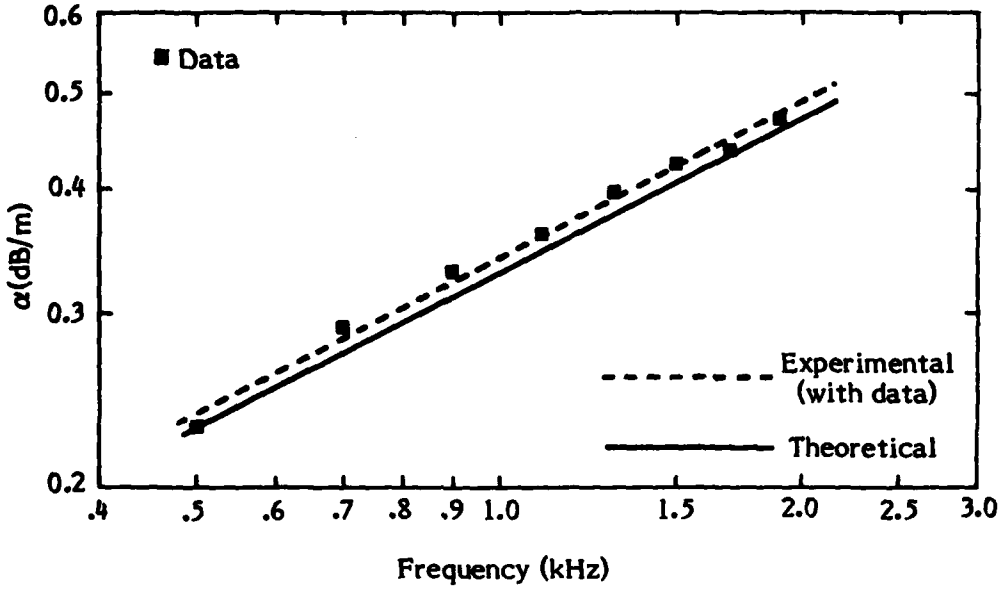

Figure 3.10

Principal mode attenuation
(comparison of theory with observed data)

ARL:UT
AS-84-593
JATC - GA
7 - 9 - 84

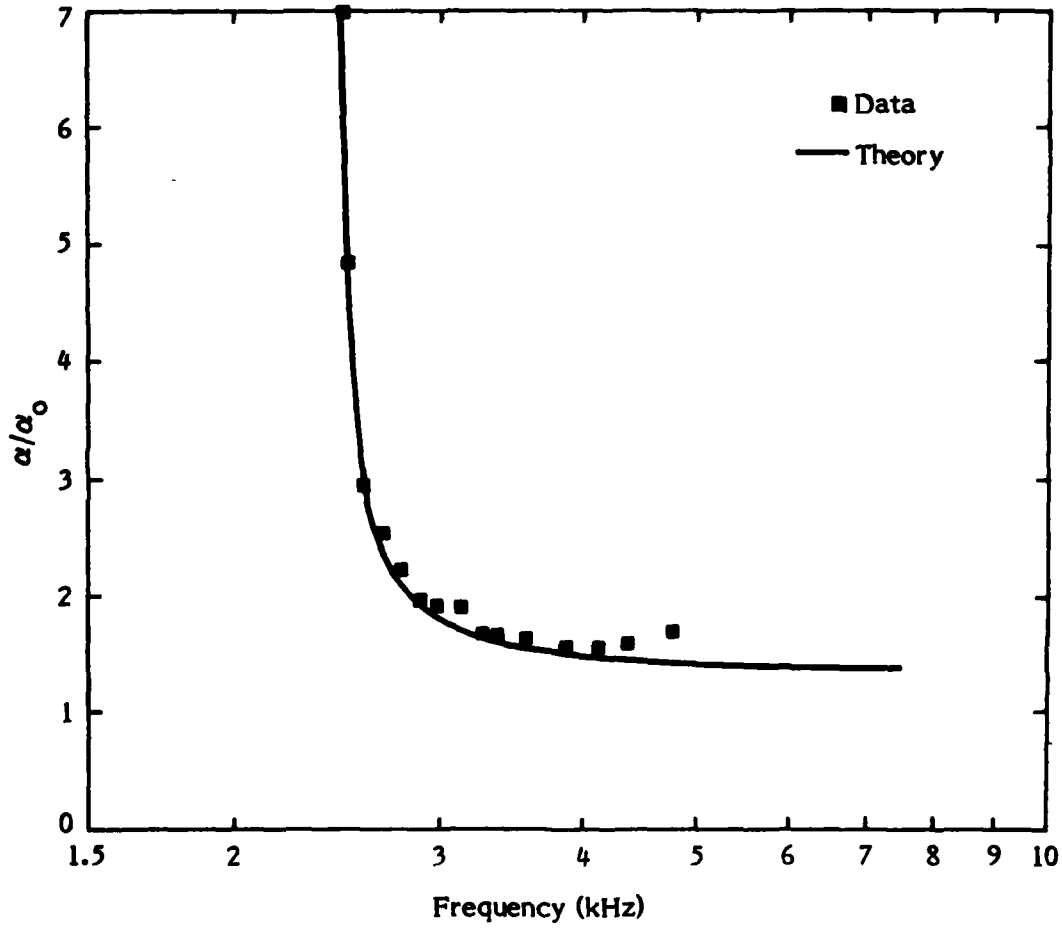

Figure 3.11

(1,0) mode attenuation
(comparison of theory with observed data)

ARL:UT
AS-84-594
JATC - GA
7 - 9 - 84

CHAPTER 4
EXPERIMENTS AND RESULTS

This chapter consists of descriptions and results of experiments which were performed to test predictions of Chapter 2. Experiments with two collinear interacting waves, called C experiments, are first to be discussed. Because collinear interaction has been observed before and is well understood, the C experiments were used to check the reliability of apparatus and experimental techniques. In one experiment we directly observed and recorded the modulated small-signal waveform. In the other we carefully checked the dependence of the weak wave suppression on the modulation index. Next, our attention turned to noncollinear interaction. Two N experiments, similar to the two collinear wave experiments, were performed first. Next, a study of the dispersive nature of noncollinear interaction was made (D experiments). Finally, the focus of the chapter turns to experiments designed to check Eq. (1.6), the proposed expression for the effective coefficient of nonlinearity (S experiments).

A. Collinear interaction experiments

1. Experiment C1

In previously reported collinear modulation experiments,[4,21,28-31] no time-domain observations of the modulation of one wave by another (as shown in Fig. 1.1) were presented. The Nicolet digital oscilloscope allows such an observation to be made quite easily. Both waves in this experiment traveled in the (0,0) mode. The pump wave was produced by a JBL-375 H driver; the weak wave was generated by the two ID-65 drivers connected in parallel and driven in phase. Probe tube scans through the waveguide--both before and during the experiment--confirmed that

only (0,0) modes were present. Each of the two waves was monitored by two B&K ¼ in. microphones and the Nicolet oscilloscope. The monitor microphone was used to observe waveforms before propagation distortion; the downstream microphone--placed at the 4.5 m port--was used to observe waveforms after propagation distortion.

The experiment was performed as follows. First, the levels of the two waves were increased to a selected sound pressure level (SPL) as measured by the monitor. Next, a waveform of the pump by itself and a combination waveform were captured and stored in the oscilloscope's memory at both microphone positions. The isolated pump waveform was digitally subtracted from the combination waveform (by using the oscilloscope's software) and the result displayed on the oscilloscope screen. The resulting waveforms showed the small-signal wave before and after interaction with the pump.

The waveforms of a typical experiment (with f_p = 800 Hz at 155 dB and f_w = 5400 Hz at 100 dB) are presented in Fig. 4.1. Because of the large difference in SPL, the combination waveform in each case shows little evidence of the presence of the weak wave. However, when the pump waveform is subtracted and the remainder vertically expanded, the small-signal wave is easily seen. At the first microphone position, where very little interaction had occurred, there is no apparent modulation of the weak wave. At the second microphone position, however, the small-signal waveform (shown in Fig. 4.1(b)) shows a very pronounced modulation.* The experiment qualitatively demonstrated the modulation of sound by sound.

*The slight irregularities that can be seen in the figure result from the inability to obtain a perfect subtraction. The acoustic signal was simply not stable enough to trigger and store the intense waveform in the exact place in the oscilloscope's memory each time.

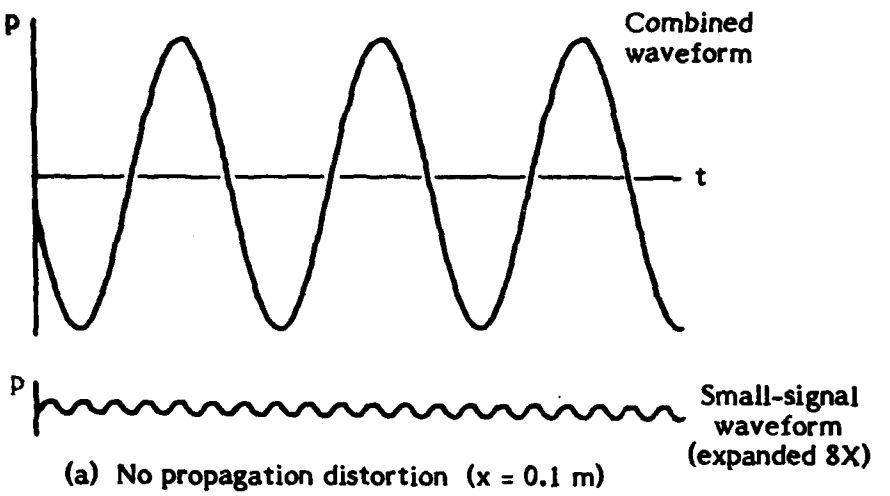

(a) No propagation distortion (x = 0.1 m)

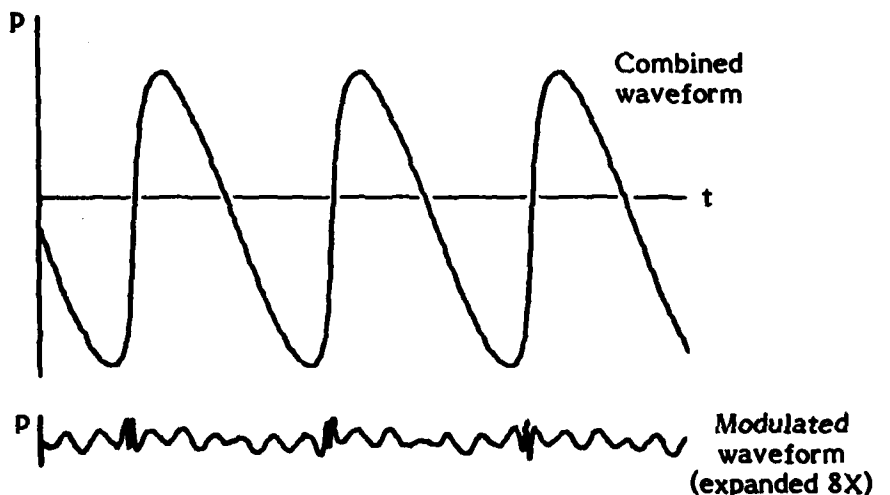

(b) After propagation distortion (x = 4.5 m)

Figure 4.1

Demonstration of the collinear modulation of sound by sound

ARL:UT
AS-84-595
JATC-GA
7-9-84

2. Experiment C2

The next experiment, intended to be a more quantitative test, was nearly identical to one done by Schaffer.[29] The main difference was that this experiment was conducted in a rectangular waveguide. As in Experiment C1, two plane waves were generated. Output from the monitor was filtered so that the two signals could be isolated from each other. The weak wave signal was used as an input to the compressor in order to keep the weak wave SPL constant; the SPL of the pump varied but was carefully controlled and measured. The downstream microphone was connected to the narrow bandpass filter (10 Hz) section of the GR 1900 wave analyzer and to the Nicolet oscilloscope.

The experiment was carried out as follows. First, values for the weak wave frequency f_w, pump frequency f_p, and the interaction distance x were chosen. Weak wave frequencies ranged from 3000 Hz to 4000 Hz, pump wave frequencies from 600 Hz to 750 Hz. The downstream microphone was placed at the 4.5 m port, and the weak wave generated. Next, the pump was turned on and its SPL (i.e., ϵ_p) gradually increased. The concurrent suppression of the weak wave was recorded. Suppression depends on the modulation index $\mu_o = \beta\epsilon_p k_w x$. Thus, the data should fall on a single curve if suppression is plotted versus μ_o, regardless of which of the several factors in μ_o are varied during the experiment. Data for our experiment were obtained by varying ϵ_p, f_w, and f_p.* The data, which are presented in Fig. 4.2, appear in horizontal clusters because they were obtained in 3 dB steps of suppression. The solid curve in the figure was computed assuming that attenuation does not affect the measured suppression, the dashed and dotted lines were computed

*There is a slight effect on the attenuation of the pump through the dependence of $\bar{\epsilon}_p$ on f_p.

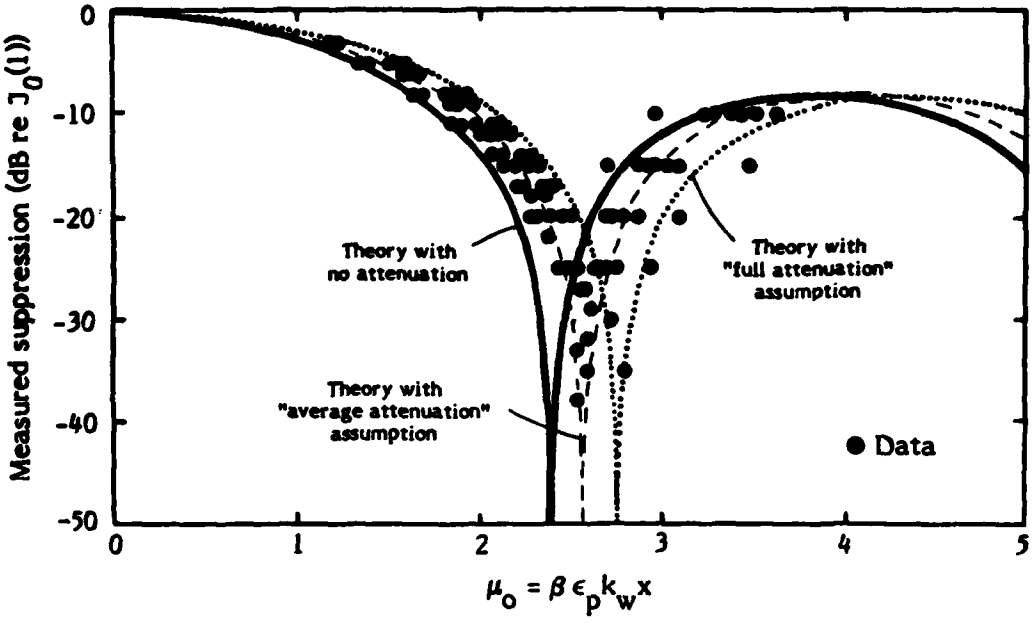

Figure 4.2

Comparison of predicted suppression of sound by sound with observed data (collinear interaction)

ARL:UT
AS-84-586
JATC - GA
7 - 9 - 84

using Schaffer's average and full-attenuation models (see Eqs. (2.36) and following). The maximum suppression observed in this experiment was about 38 dB and is comparable to the suppressions obtained by Schaffer and Gong, Zhu, and Du.[30] The data fall nicely between the two outer curves and thus generally verify the theory. Schaffer's "average attenuation" model seems to offer the best single fit.

B. Noncollinear interaction experiments

The excellent results obtained from the collinear interaction experiments indicated that our apparatus and techniques were reliable. We now turn our attention to noncollinear experiments.

1. Experiment N1

A qualitative experiment was performed to see whether the modulation of sound by sound could be directly observed for the noncollinear interaction of two waves. The experimental procedures for this experiment were quite simila to those described for Experiment C1. However, there were a few changes. First, the University drivers were connected out of phase in order to excite the (1,0) mode. Next, the measurement microphone was moved to the 2.7 m port, since maximum suppression of the weak wave was predicted to occur at that point (see Fig. 2.3). Numerous probe tube scans were made in this experiment. However, instead of checking for only (0,0) modes (as in the collinear experiment), the probe tube was used to confirm the (1,0) mode's presence as well.

The results of the experiment are shown in Fig. 4.3. For the weak wave the frequency was 6600 Hz and the SPL 100 dB; for the pump wave the frequency was 700 Hz and the SPL 152 dB. As noted in the discussion of the collinear experiments the slight irregularities and amplitude changes which appear in the

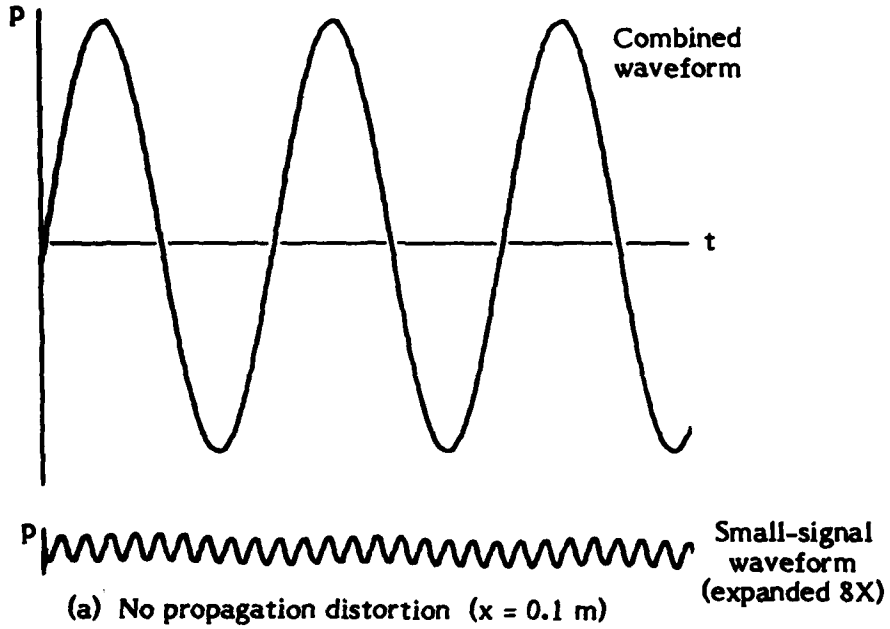

(a) No propagation distortion (x = 0.1 m)

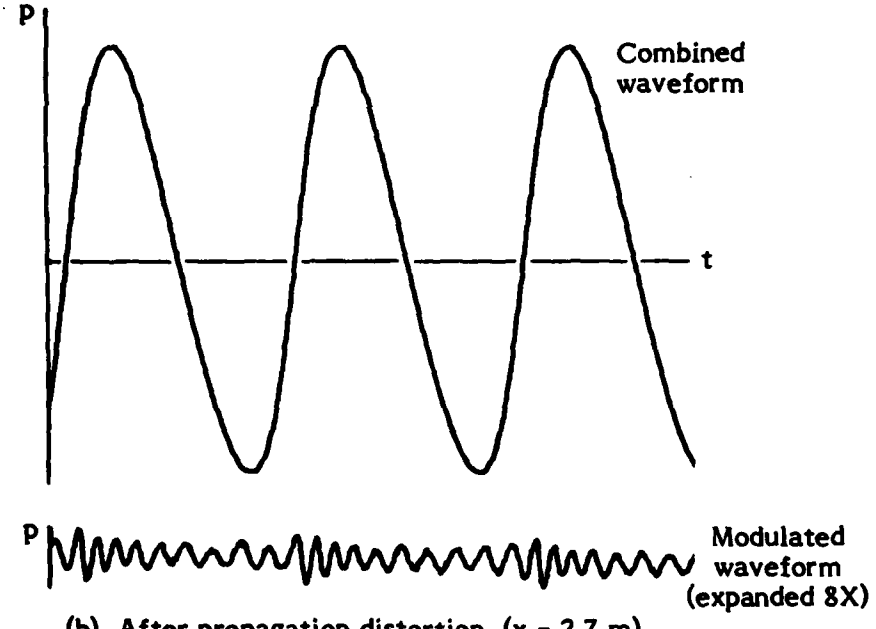

(b) After propagation distortion (x = 2.7 m)

Figure 4.3

Demonstration of the noncollinear modulation of sound by sound

modulated wave are a result of the inability to match the two waveforms exactly before finding their difference. In spite of the irregularities, however, the modulation is still quite apparent.

2. Experiment N2

Experiment N2 provided a frequency domain view of distortion and modulation. Instead of measuring waveforms, we measured spectra. Most of the apparatus was the same as in Experiment N1. The measurement microphone was connected to the HP 3580A spectrum analyzer rather than to the Nicolet oscilloscope. The frequencies of the (0,0) and (1,0) modes were 900 Hz and 6700 Hz, respectively. The downstream microphone was placed at the 2.1 m port. Spectra were then obtained as a function of SPL_p.

The series of spectrum analyzer photographs obtained are presented in Fig. 4.4. Tic marks on the vertical scales show 10 dB increments. The weak wave component and sidebands have been shaded for clarity. Notice the harmonic distortion of the pump. For this series of photographs the value of σ_p varied from 0.11 at the lowest pump level (140 dB) to 0.49 at the highest pump level (153.3 dB). The maximum suppression attained was only about 20 dB and occurred at a value of $SPL_p \doteq 153$ dB. Although the amount of suppression was not comparable to that seen in the collinear experiments, the experiment nicely shows that suppression does occur, even when the interaction is noncollinear.

3. Experiment N3

We now discuss an experiment designed to examine the dependence of the suppression on the noncollinear modulation index, which is much more complicated than the index for collinear interaction (cf. Eq. (2.12) with Eq. (2.23)). In particular,

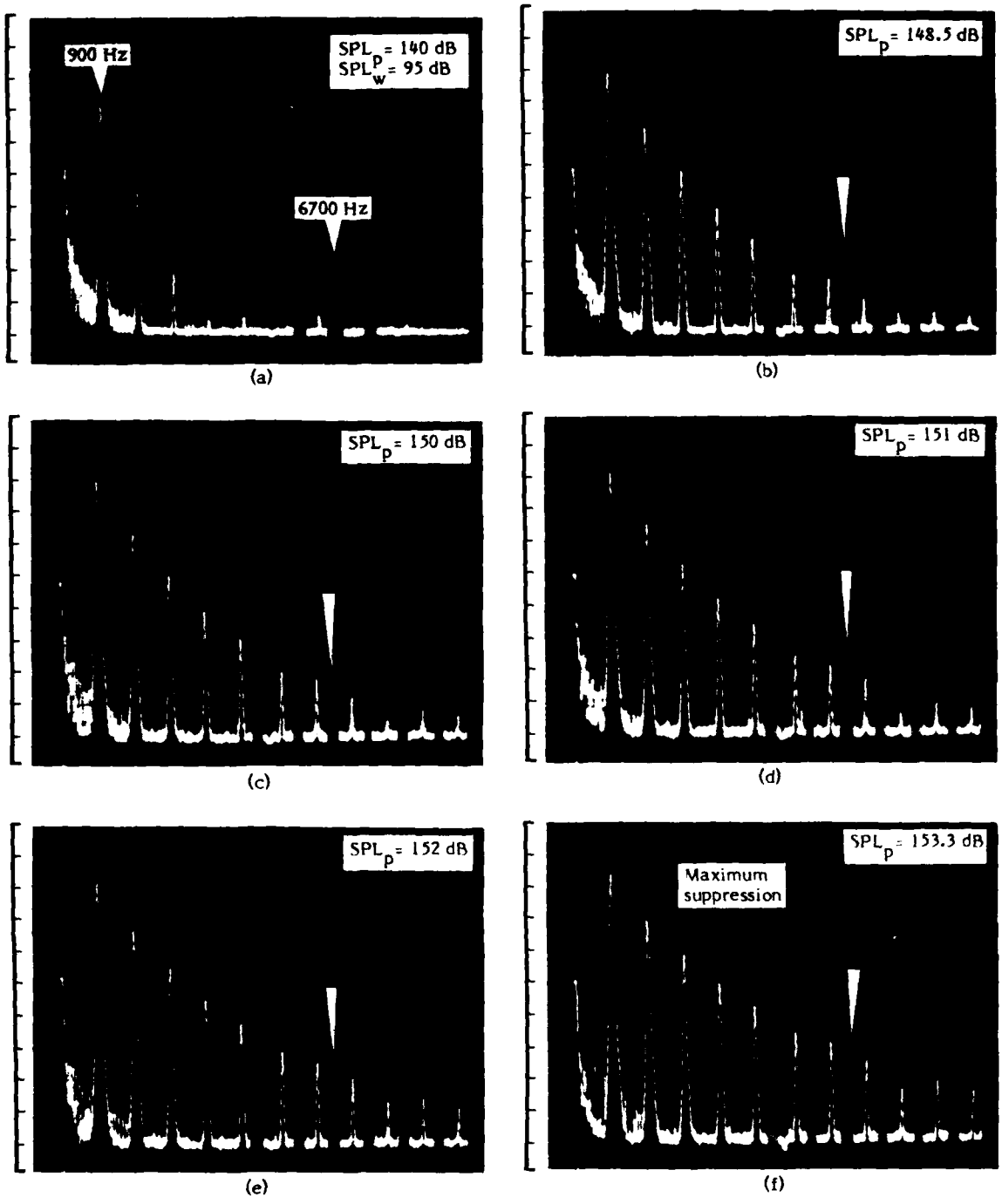

Figure 4.4

Observation of the modulation of sound by sound in the frequency domain

because of geometric dispersion, suppression now depends strongly on f_p. Moreover, the variation in suppression is periodic with interaction distance (recall Fig. 2.3).

The experiment was performed with the same apparatus used in Experiment C2. The weak wave was, of course, generated in the (1,0) mode rather than in the (0,0) mode. The range of the pump frequencies used was 500 Hz to 700 Hz; for the weak wave the range was 5 kHz to 7 kHz. The measurement procedure was the same as that in Experiment C2.

The data are presented in Fig. 4.5. In general, they do not agree well with the theoretical curves. The most plausible explanation is as follows: To achieve any appreciable (i.e., greater than 10 dB) suppression of the weak wave, either extremely high values of ϵ_p or f_w are required. Unfortunately, extremely high values of ϵ_p could not be attained with the JBL drivers. Consequently, high weak wave frequencies--above the cut-on frequencies of undesired modes--were necessary. Using a probe tube, we were able to confirm the propagation of one of these modes--the (0,1)--during many of the experiments. The presence of modes not accounted for in the theory may be an explanation for the erroneous results.

C. Geometric dispersion experiments

The results from the last experiment indicated that the use of suppression as a "null detector" is not a practical means of measuring the θ dependence of β_{eff}. A different experimental approach would be needed. However, before deciding on a particular experiment, we decided to examine another aspect of the interaction, geometrical dispersion. Armed with a better understanding of the interplay of the waves within the waveguide, we could then proceed with our study.

1. Experiment D1

We devised an experiment to check the predictions presented in Fig. 2.3. To avoid unwanted modes, we chose the value of the (1,0) mode frequency well

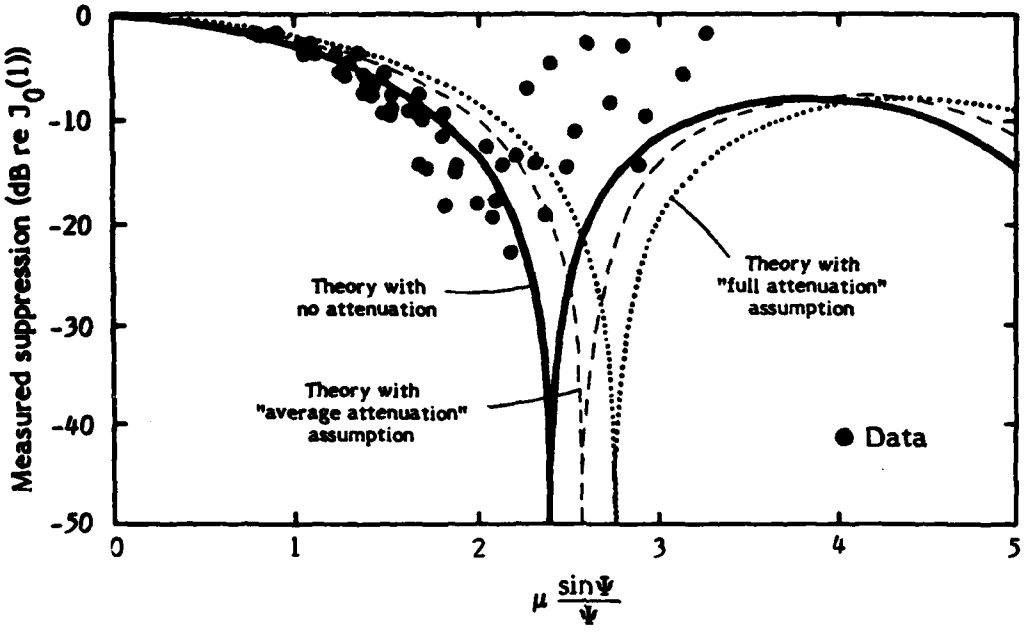

Figure 4.5

Comparison of predicted
suppression of sound by sound
with observed data
(noncollinear interaction)

ARL:UT
AS-84-598
JATC - GA
7 - 9 - 84

below the cut-on frequency of the (0,1) mode. The (0,0) and (1,0) modes were turned on and a measure of the SPL of the primary weak wave component as a function of distance was made. Data were corrected for attenuation and plotted.

Figure 4.6 shows the results of two sets of measurements. The frequencies used are shown in the figure. Unfortunately, since the weak wave's frequency was low and the maximum level of the pump wave was limited, only small amounts of suppression are evident in these plots. Even at these small suppressions, however, the data do exhibit a periodicity and compare favorably with the theoretical curves shown for these frequencies.

2. Experiment D2

The behavior of the sum and difference frequency components (first order sidebands) as a function of interaction distance is also of interest (especially in light of the differences between Hamilton's predictions and those of Chapter 2). The relative levels of the sum and difference frequency components were measured as a function of distance. The results are presented in Fig. 4.7. The values of SPL_+ and SPL_- at the first peaks were 73 dB and 69 dB, respectively. The solid curve shown in the figure is based on Hamilton's predictions (Eq. (B.9)), the dashed curve on FM theory. As in Experiment D1, the data have been corrected for attenuation. As the plots show, Hamilton's predictions are in excellent agreement with the data. Although FM theory accurately predicts the behavior of the weak wave component, it does not do as well with these two sidebands. It may, however, be argued that the condition $\omega_p << \omega_w$ was not met in the D experiments.

D. 3dB suppression experiments

Two important lessons were learned from the N and D1 experiments. First, the presence of undesired modes may lead to results which cannot be

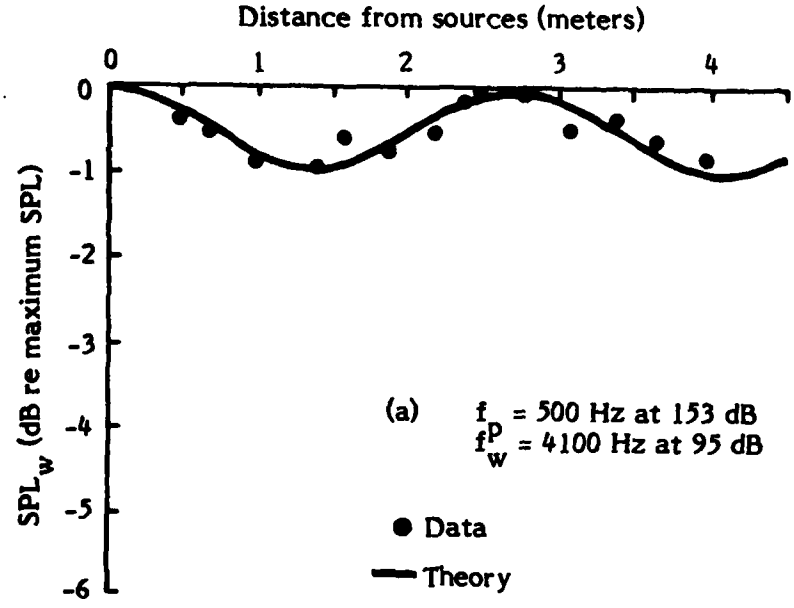

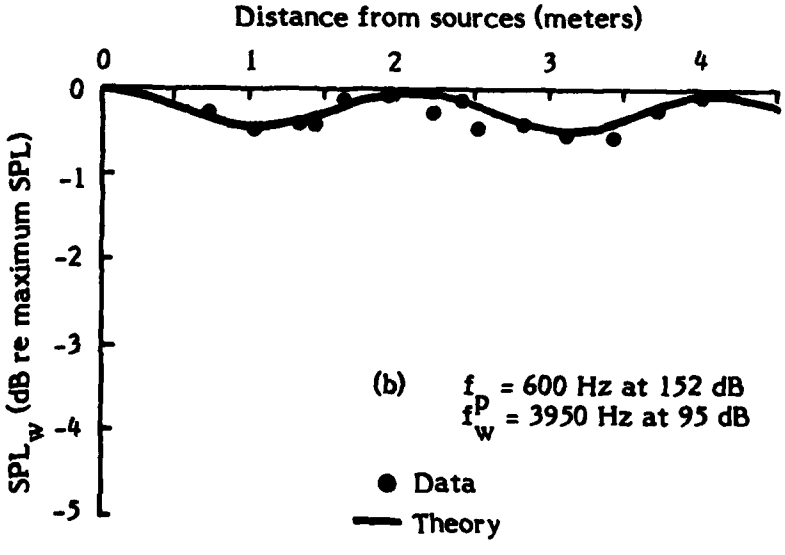

Figure 4.6

Demonstration of geometric dispersion in a waveguide (weak wave component)

ARL:UT
AS-84-599
JATC - GA
7 - 9 - 84

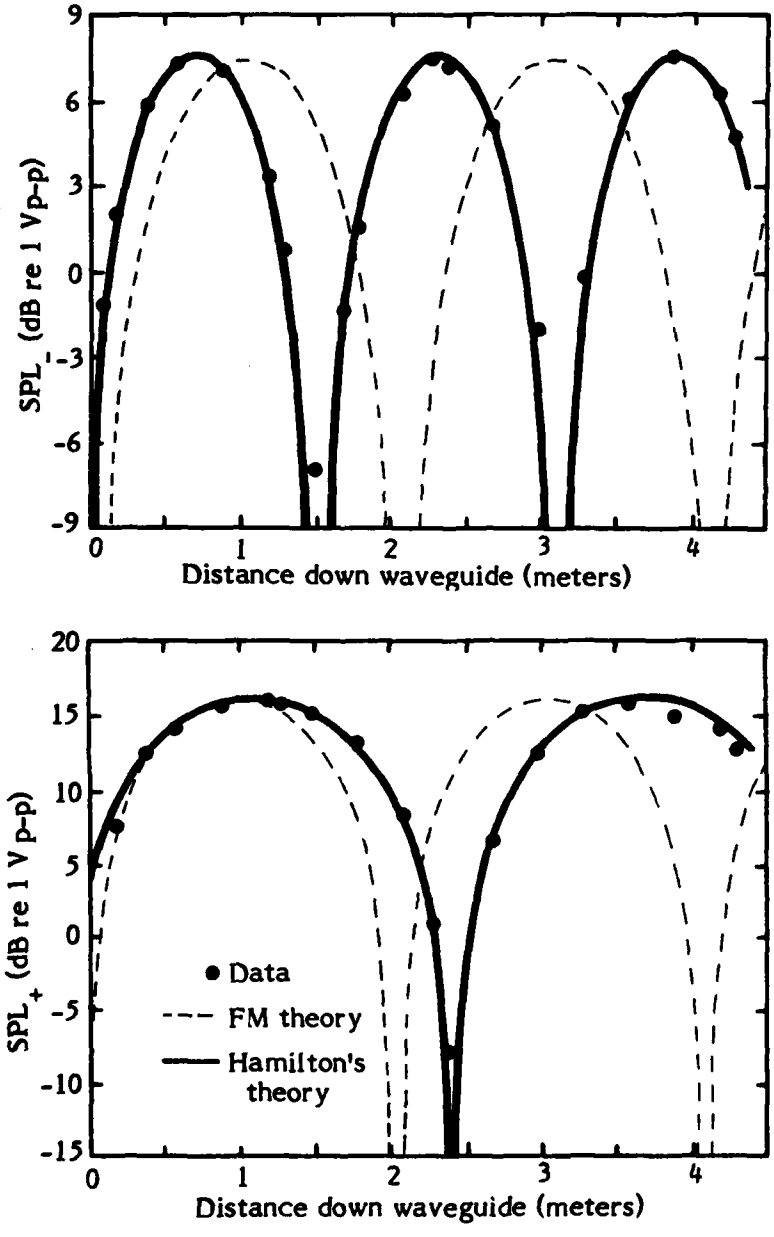

Figure 4.7

Comparison of observed data with predicted periodicity of the sum and difference frequency wave amplitudes

f_p = 600 Hz

f_w = 3950 Hz

ARL:UT
AS-84-600
JATC-GA
7-9-84

interpreted. Weak wave frequencies must thus be chosen below the (0,1) cut-on frequency. Second, only moderate suppression of the weak wave component may be achieved with the pump levels available to us. An experiment was therefore devised requiring a suppression of only 3 dB. Results of these experiments make up the final topic of this chapter.

If the pump frequency and interaction distance are fixed, the only variables in the modulation index are the weak wave frequency and the level of the pump wave. The procedure in each of the following experiments was to set f_w and vary SPL_p until exactly 3 dB of suppression was achieved. Pump level was then plotted against weak wave frequency for 3 dB suppression. By comparing the measured curves with theoretical predictions we hoped to deduce the form of the effective nonlinearity coefficient.

The apparatus and procedure for each experiment were as follows. The monitor microphone was used to measure source levels of the intense and weak waves, the downstream microphone was used to measure the level of the weak wave and the amount of suppression. The latter microphone was connected to the filter section of the GR wave analyzer and then to an attenuator (HP-350C or GR-1450 TB) and the Nicolet oscilloscope. The experiment was begun by turning on the weak wave (by itself) at a selected frequency f_w. A constant source level was maintained by using the BFO and compressor (AGC) circuits of the B&K heterodyne analyzer. The level seen on the Nicolet oscilloscope was next reduced 3 dB with the use of an attenuator. The attenuated signal was then stored on the oscilloscope display as a visual reference and the attenuator removed. The pump wave was turned on and its SPL increased until the amplitude of the weak wave signal was suppressed to the 3 dB reference level displayed on the oscilloscope. The SPL of the pump was

recorded, another weak wave frequency selected, and the entire process repeated. The results for three values of pump wave frequency--500 Hz, 450 Hz, and 400 Hz--and two different measurement positions are shown in Figs. 4.8 through 4.10. Each experiment is now discussed.

1. Experiment S1

Figure 4.8 shows the data for x=1.8 m and f_p=500 Hz and also two theoretical curves. Different symbols indicate data obtained during different runs. The frequency of the (1,0) mode was chosen between 4.3 kHz and 4.9 kHz; accordingly, the angle of intersection varied from 36° to 30°. At the lower end of the frequency range the solid theoretical curve ($\beta_{eff}=\cos\theta+\frac{\gamma-1}{2}$) is confirmed. Two drops of the data then apparently spoil confirmation. There are, however, explanations for these drops. The first drop (and gap), in the vicinity of 4.5 kHz, is associated with the nearness of the weak wave frequency to the ninth harmonic of the intense wave. Near a harmonic, (1,0) modal purity was observed to deteriorate. Furthermore, the harmonic in the (0,0) mode cannot easily be filtered out. The second drop, which is more pronounced, occurs at frequencies near 4.6 kHz, which is the cut-on frequency of the (0,1) mode. The presence of the (0,1) mode was easily confirmed with a probe tube scan. However, the mode became less apparent as the weak wave frequency was raised. In fact, above 4.7 kHz the (0,1) mode could no longer be detected.

It is significant that between 4.7 kHz and 4.9 kHz the trend of the data is back toward the solid theoretical curve. Near 4.9 kHz yet another unwanted mode, the (2,0), appeared. The two theoretical curves in the figure (the thick solid and dashed lines) have been plotted using Schaffer's average attenuation model. Theoretical curves using the other two attenuation assumptions are only slightly

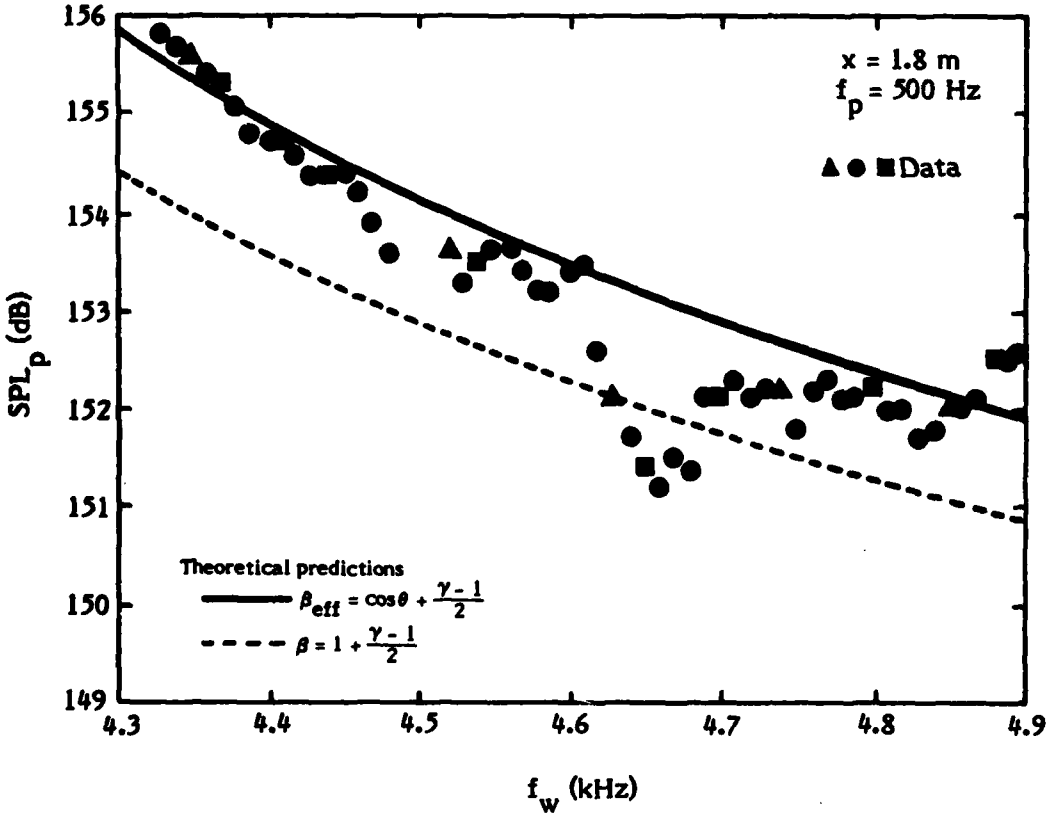

Figure 4.8

Comparison of observed data with predicted SPL_p for 3 dB weak wave suppression (f_p = 500 Hz)

ARL:UT
AS-84-601
JATC - GA
7 - 9 - 84

different and are not plotted. For this experiment the data seem to support the theoretical prediction that $\beta_{eff}=\cos\theta + \frac{\gamma-1}{2}$.

2. Experiment S2

Figure 4.9 represents the data for f_p=450 Hz and x=1.8 m. Here the weak wave frequency lay in the range 4.1 kHz to 4.9 kHz, which corresponds to angles of intersection from 38° to 30°. The drops evident in the previous data, caused by the presence of the (0,1) mode and the pump wave harmonic, are not as apparent in these data. Even so, the (0,1) mode was detected with a probe tube scan at frequencies from 4.6 kHz to about 4.7 kHz. The data presented here seem to support the solid curve at lower weak wave frequencies and begin to tend toward the dashed curve near the center of the plot. This tendency may be the result of the (0,1) mode's presence. Indeed, when the weak wave frequencies were high enough that the (0,1) mode disappeared, the data tended back toward the solid curve.

3. Experiment S3

The final set of data was obtained at a pump wave frequency of 400 Hz and a measurement position of 2.1 m. The data are shown in Fig. 4.10. The frequency of the (1,0) mode was again selected between 4.1 kHz to 4.9 kHz (angles between 38° and 30°). The (0,1) mode was detected at weak wave frequencies from 4.5 kHz to about 4.7 kHz. The data presented in this figure exhibit trends comparable to those in Figs. 4.8 and 4.9. At low values of f_w, the data fit well with the solid line theoretical prediction. The fit is also good at the high end of the f_w range. The weakness in the center range of f_w, especially apparent in this experiment, seems to be associated with the cut-on of the (0,1) mode.

The possible sources of error in the latter three experiments may be of interest. By far the largest possible error is in the measurement of the pump wave's

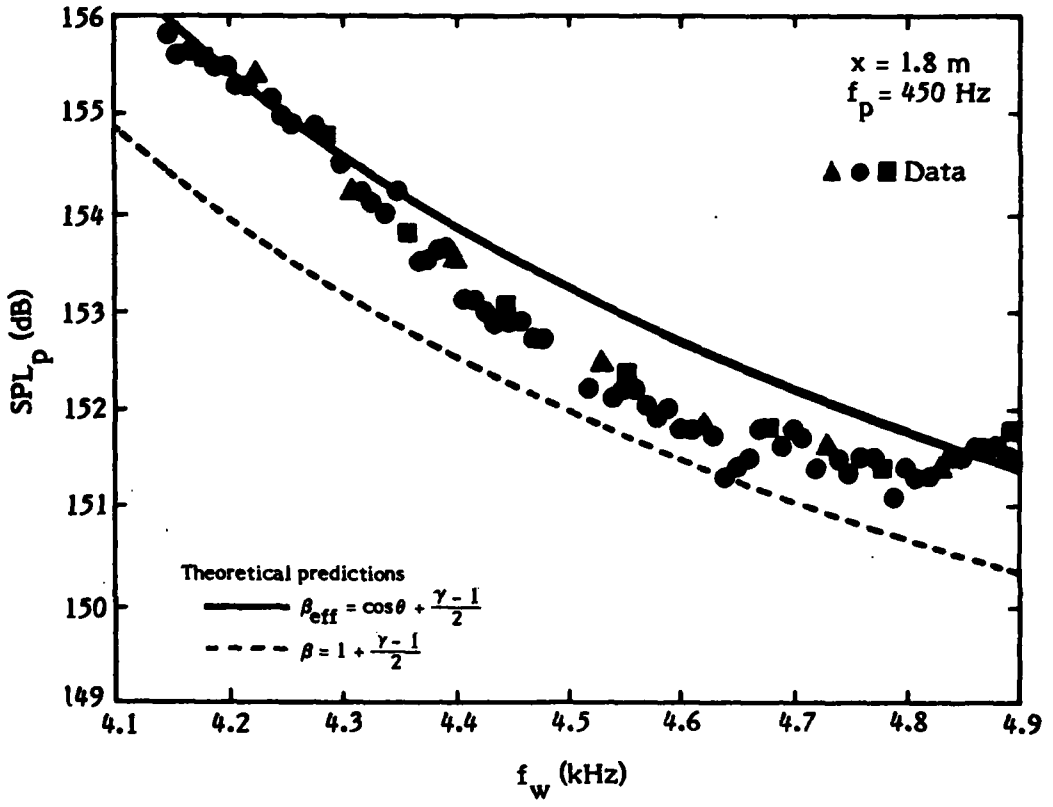

Figure 4.9

Comparison of observed data with predicted SPL_p for 3 dB weak wave suppression (f_p = 450 Hz)

ARL:UT
AS-84-602
JATC - GA
7 - 9 - 84

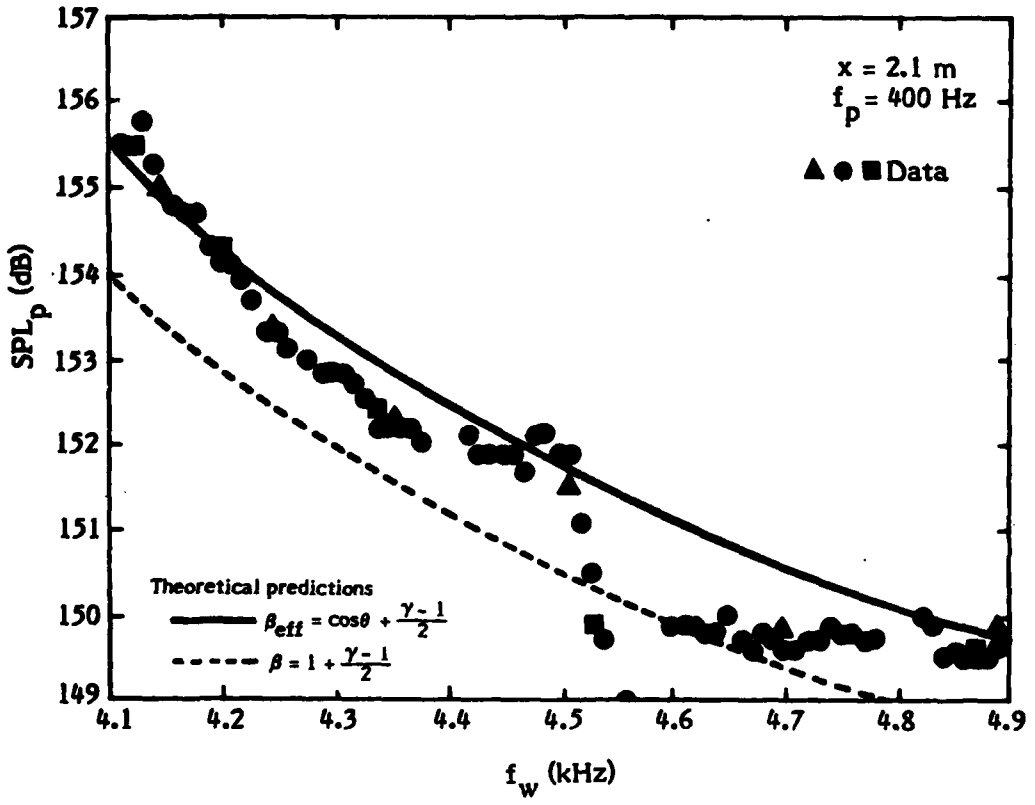

Figure 4.10

Comparison of observed data with predicted SPL$_p$ for 3 dB weak wave suppression (f_p = 400 Hz)

ARL:UT
AS-84-603
JATC - GA
7 - 9 - 84

SPL and the calculation of ϵ_p. The error involved in this measurement is judged to be small ($\pm$0.3 dB). All the equipment used for measurement purposes had been recently calibrated (by B&K personnel) or directly compared with calibrated equipment. Furthermore, temperatures and atmospheric pressures were carefully monitored during each experiment and the appropriate corrections in the reference level made. The calibration techniques were therefore accurate. Another possible source of error was the determination of the interaction length and, therefore, the placement of the theoretical curves. This error is complicated by the fact that the interaction region may begin nearer to (or farther from) the sources than assumed depending on the combination of source frequencies. For our experiments the interaction length was measured from the monitor position. From various experiments an estimate of the size of the error was set at $\pm$0.2 m. It should be noted that an error of this magnitude would slightly change the slope of each theoretical curve shown in Figs. 4.8 through Fig. 4.10. General conclusions and final comments are the topics of the next and concluding chapter.

CHAPTER 5
CONCLUSIONS

A mainly experimental study of the nonlinear interaction of noncollinear waves in a rectangular waveguide has been carried out. A finite-amplitude wave (pump) traveling in the (0,0) mode modulates a weak wave traveling in the (1,0) mode. The results of the interaction are sideband generation and a suppression of the weak wave primary. The theoretical amplitude of the weak wave was based on the assumption that the interaction in the waveguide is the same as that of two infinite plane waves intersecting in an open medium. New considerations caused by the noncollinearity are (1) the angular dependence of β_{eff}, and (2) geometric dispersion. The latter was found to dominate the interaction.

Various experiments were performed. First, two collinear experiments were performed to check our experimental technique and to observe the modulation and suppression of sound by sound. Next, noncollinear experiments were performed. The first two were carried out to observe qualitatively the modulation for noncollinear waves. Other experiments were done to test the effect of geometric dispersion. Finally, three experiments, which were used to test the prediction $\beta_{eff} = \cos\theta + \frac{\gamma - 1}{2}$, concluded our study.

Results of the experiments and conclusions drawn are as follows. The collinear modulation and suppression of sound by sound experiments were a complete success. We stored actual waveforms of a few modulated waves and obtained excellent agreement between the theoretical predictions and observed data. In one experiment we obtained a 38 dB suppression of the primary component of the weak wave. We were also able to obtain and store a few modulated waveforms for noncollinear interaction. The experiments performed to examine geometric dispersion confirmed the theory describing this aspect of the interaction. The

experiments done to examine the angular dependence of β_{eff} were, however, beset with a few difficulties. The presence of an unwanted higher order mode (the (0,1) mode) and a pump harmonic had a significant effect on the data. Limited source output also hindered measurements. These two problems restricted the angle of interaction to a small range (30° to 38°). Even so, the data do seem to support the prediction that $\beta_{eff} = \cos\theta + \frac{\gamma - 1}{2}$.

A few changes which might improve the noncollinear experiments are now considered. One solution is to use drivers capable of much higher output. An alternative, of course, is to use two or more of the JBL drivers. The gains, however, are slight. A 6 dB increase in maximum pump wave SPL extends the range of the angle of intersection only about 6°. By using a smaller waveguide, we might improve our experiments a bit more. We must keep $\omega_p << \omega_w$ if FM theory is to be accurate. With a smaller waveguide the cut-on frequency of the (1,0) mode is higher, and thus the requirement $\omega_p << \omega_w$ is easier to maintain. Moreover, a waveguide of smaller cross-section also makes it easier to achieve a greater pump SPL.

Two other changes we consider concern the elimination of unwanted modes. Perhaps the most annoying aspect of the data presented in Figs. 4.8 through 4.10 is the effect the (0,1) mode had on the interaction. In our experimentation there was some indication that the (0,1) mode may be generated primarily at the sources. One or both of the following schemes may improve the results. A smoother transition between driver and waveguide is one solution. An alternative may be the use of a mode filter (see, for example, Said[52]). The first meter or so of the inside of the waveguide could be lined with an absorptive material. However, the material need only be put on the two walls on which the (0,1) mode bounces.

The (1,0) mode is thus unaffected. The effect of the extra absorption on the (0,0) mode might, however, prove troublesome.

The improvements we have discussed may prove helpful. As we have seen, however, the angular dependence of β_{eff} still has only a small effect on noncollinear interaction. Indeed, the most important conclusion we have made is that geometric dispersion is the dominant factor in noncollinear interaction. The results of this investigation may therefore be the best we can obtain using the techniques of this study.

AD-A144 440 NONLINEAR INTERACTION OF TWO NONCOLLINEAR SOUND WAVES IN A RECTANGULAR WAVEGUIDE(U) TEXAS UNIV AT AUSTIN APPLIED RESEARCH LABS J A TEN CATE JUN 84 ARL-TR-84-16 2/2

UNCLASSIFIED N00014-75-C-0867 F/G 20/14 NL

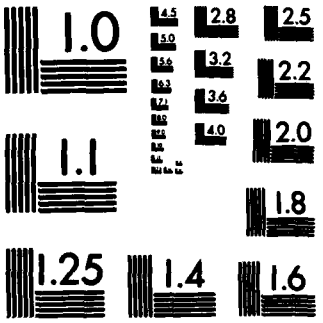

APPENDIX A

TRAVEL DIRECTIONS OF SUM AND DIFFERENCE FREQUENCY WAVES

In this appendix we demonstrate that the sum and difference frequency waves travel in the same direction as the weak wave primary whenever $\omega_w \gg \omega_p$. We begin with the FM theory expression for the amplitude of the sum and difference frequency components, Eq. (2.26). In complex form the equation is

$$\left|\frac{u_{\pm}}{u_{ow}}\right| = \left| J_1\left(\mu\frac{\sin\Psi}{\Psi}\right) \mathrm{Im}\left\{e^{i\left[\omega_{\pm}\tau' + k_p r(1-\cos\theta)/2\right]}\right\}\right| , \qquad (A.1)$$

where $\omega_{\pm} = \omega_w \pm \omega_p$ and, as in Chapter 2, $\tau' = t - r/c_o$. The complex exponential may be written in terms of t and r as

$$e^{i\left[\omega_{\pm}\tau' + k_p r(1-\cos\theta)/2\right]} = e^{i\omega_{\pm}\left(t - \left[\frac{\omega_{\pm}}{\omega_{\pm} c_o} - \frac{\omega_p}{\omega_{\pm} c_o}(1-\cos\theta)/2\right] r\right)} . \qquad (A.2)$$

We now define $\eta_{\pm}$ to be the spatial coordinates in the direction of the sum or difference frequency wave. Likewise, we define $\alpha_{\pm}$ to be the angles the two waves make with the x-axis (see Fig. 2.2)

$$x = \eta_{\pm}\cos\alpha_{\pm} \quad . \qquad (A.3)$$

Since $x = r\cos\theta$, Eq. (A.3) may be written in terms of $\eta_{\pm}$, $\alpha_{\pm}$, and θ,

$$r = \frac{\eta_{\pm}\cos\alpha_{\pm}}{\cos\theta} \quad . \qquad (A.4)$$

The right-hand side of Eq. (A.2) thus becomes

$$e^{i\omega_{\pm}\left\{t - \left(\frac{\cos\alpha_{\pm}}{\cos\theta}\right)\left[\frac{\omega_p}{\omega_{\pm}c_o} - \frac{\omega_p}{\omega_{\pm}c_o}(1 - \cos\theta)/2\right]\eta_{\pm}\right\}} \quad .$$

Since the sound speed in the direction of $\eta_{\pm}$ is simply c_o, the coefficient of $\eta_{\pm}$ may be set equal to $1/c_o$. After some manipulation, we obtain

$$\cos\theta = \left[1 - \frac{\omega_p}{\omega_{\pm}}(1-\cos\theta)/2\right]\cos\alpha_{\pm} \quad . \tag{A.5}$$

One of the assumptions of the theory presented in Chapter 2 is that $\omega_w \gg \omega_p$. Given this assumption, one has $\frac{\omega_p}{\omega_{\pm}} \doteq \frac{\omega_p}{\omega_w} \rightarrow 0$ and Eq. (A.5) becomes

$$\cos\theta = \cos\alpha_{\pm} \quad . \tag{A.6}$$

Thus, whenever $\omega_w \gg \omega_p$, the sum and difference frequency waves propagate in the same direction as the weak wave.

APPENDIX B

GEOMETRIC DISPERSION VIA WESTERVELT'S INHOMOGENOUS WAVE EQUATION

The following derivation was carried out by M. F. Hamilton and originated, in part, from his study of the effects of dispersion on the parametric array.[53] In the following analysis, the interaction of two noncollinear plane waves is considered. Hamilton's approach is based on Westervelt's inhomogeneous wave equation[54] and is similar to that described by Zverev and Kalachev.[55] Since the interaction Hamilton examines is nearly identical to the one in our investigation, his results may be applied to our problem. In particular, his analysis yields predictions for the periodicity of the amplitudes of the sum and difference frequency waves in the waveguide. These predictions differ from those presented in Chapter 2. The results of our analysis are derived with the assumption that $\omega_w >> \omega_p$. Hamilton, however, makes no such assumption. On the other hand, Hamilton's results are valid only for weak pump waves, whereas ours are derived without restricting the strength of the pump. It is encouraging that both results agree for overlapping conditions, i.e., $\omega_w >> \omega_p$ and a weak pump wave.

The analysis begins with Westervelt's inhomogeneous wave equation. In terms of pressure it can be expressed as

$$\nabla^2 p - \frac{1}{c_o^2} \frac{\partial^2 p}{\partial t^2} = - \rho_o \frac{\partial q}{\partial t} , \qquad \text{(B.1)}$$

where the source strength q is given by

$$q = \frac{\beta_{eff}}{\rho_o^2 c_o^4} \frac{\partial}{\partial t}(p^2) \quad , \tag{B.2}$$

and

$$\beta_{eff} = \cos\theta + \frac{\gamma - 1}{2} . \tag{B.3}$$

Note that Eq. (B.3) is the same as Eq. (1.6). To solve Eq. (B.1), we may utilize the method of successive approximations. As a first approximation, the right-hand side (which contains only nonlinear terms) is assumed to be small and may thus be ignored. A solution of the resulting approximate wave equation which satisfies the boundary condition

$$p(0,t) = P_1 e^{i\omega_1 t} + P_2 e^{i\omega_2 t} \quad ,$$

is

$$p = P_1 e^{i(\omega_1 t - \vec{k}_1 \cdot \vec{r})} + P_2 e^{i(\omega_2 t - \vec{k}_2 \cdot \vec{r})} \quad , \tag{B.4}$$

where P_1 and P_2 are the peak pressure amplitudes of the two waves and $\vec{k}_1$ and $\vec{k}_2$ are the primary wave vectors as shown in Fig. B.1. Equation (B.4) is the first approximation. If this equation is substituted into the right-hand side of Eq. (B.1), the solution of the resulting equation is the second approximation. It is this solution we now seek.

The wave equation which results from the substitution of Eq. (B.4) into Eq. (B.1) has a source function composed of four different terms--two at the second harmonic frequencies, one at the sum (+) frequency, and one at the difference (-) frequency. By considering only the sum and difference frequency terms, we obtain a new source function $q_{\pm}$ given by

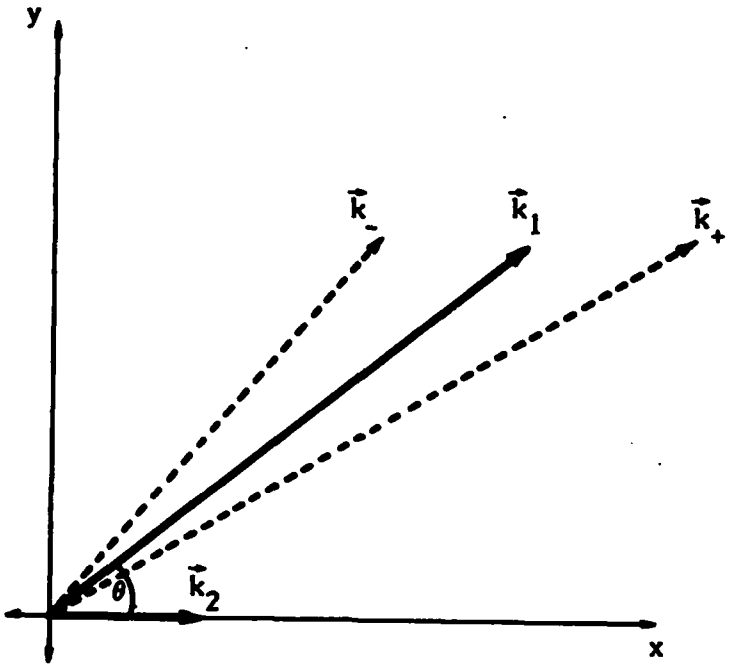

Figure B.1

Primary, sum, and difference frequency wave vectors

ARL:UT
AS-84-604
JATC-GA
7-9-84

$$q_{\pm} = P_1 P_2 \frac{\beta_{eff}\, \omega_{\pm}^2}{\rho_o c_o^4} e^{i(\omega_{\pm} t - \vec{k}_{\pm} \cdot \vec{r})} \quad , \tag{B.5}$$

where $\vec{k}_{\pm} = \vec{k}_1 \pm \vec{k}_2$ (the vector sum and difference of the primary wave vectors shown in Fig. B.1) and $\omega_{\pm} = \omega_1 \pm \omega_2$. Using the transform

$$f_{\omega}(x,y,z) = \int_{-\infty}^{\infty} f(x,y,z,t)\, e^{-i\omega t}\, dt \quad ,$$

we may express the wave equation in the frequency domain as

$$\nabla^2 p_{\omega_{\pm}} + \chi_{\pm}^2 p_{\omega_{\pm}} = C e^{-i\vec{k}_{\pm} \cdot \vec{r}} \quad , \tag{B.6}$$

where

$$p_{\omega_{\pm}}(x,y,z) = \int_{-\infty}^{\infty} p(x,y,z,t)\, e^{i\omega_{\pm} t}\, dt$$

and $\chi_{\pm} = \frac{\omega_{\pm}}{c_o}$ and $C = \beta_{eff}\, \omega_{\pm}^2 \frac{P_1 P_2}{\rho_o c_o^4}$. If $\eta_{\pm}$ is defined to be along the direction of propagation of the sum and difference frequency waves, then $\vec{k}_{\pm} \cdot \vec{r} = k_{\pm} \eta_{\pm}$ where $k_{\pm} = |\vec{k}_{\pm}|$. The Laplacian in Eq. (B.6) may thus be replaced by $\frac{\partial^2}{\partial \eta_{\pm}^2}$ and the wave equation becomes

$$\left(\frac{\partial^2}{\partial \eta_{\pm}^2} + \chi_{\pm}^2 \right) p_{\omega_{\pm}} = C e^{-ik_{\pm}\eta_{\pm}} \quad . \tag{B.7}$$

With the boundary condition $p_{\omega_{\pm}}(\eta_{\pm} = 0) = 0$, the solution of Eq. (B.7) is

$$p_{\omega_{\pm}} = \frac{C}{\chi_{\pm}^2 - k_{\pm}^2} \left[e^{-ik_{\pm}\eta_{\pm}} - e^{-i\chi_{\pm}\eta_{\pm}} \right]$$

or

$$p_{\omega_\pm} = \frac{iC\eta_\pm}{\chi_\pm + k_\pm} e^{-i\frac{\chi_\pm + k_\pm}{2}\eta_\pm} \left[\frac{\sin \frac{\chi_\pm - k_\pm}{2}\eta_\pm}{\frac{\chi_\pm - k_\pm}{2}\eta_\pm} \right] .$$

In the collinear case $\chi_\pm = k_\pm$ and $p_{\omega_\pm}$ grows linearly with η_+ or η_-. However, if $\chi_\pm \neq k_\pm$, the magnitude of the pressure of the sum or difference frequency is periodic. The period, in fact, is determined by the periodicity of the sine function and is given by

$$\Delta\eta_\pm = \frac{2\pi}{\chi_\pm - k_\pm} . \tag{B.8}$$

The above analysis is now applied to the propagation of two waves in a waveguide. The wave vectors are chosen so that $\vec{k}_1 = \vec{k}_w$ and $\vec{k}_2 = \vec{k}_p$ (the directions are shown in Fig. B.1). With this geometry Eq. (B.8) may be rewritten in an alternative form as

$$\Delta\eta_\pm = \frac{2\pi}{(k_w \pm k_p) - \xi_\pm} , \tag{B.9}$$

where $\xi_\pm = \sqrt{k_w^2 + k_p^2 \pm 2k_w k_p \cos\theta}$ and θ is the angle of intersection between $\vec{k}_w$ and $\vec{k}_p$.

If the frequency of one of the waves is much higher than that of the other wave, Eq. (B.9) should reduce to Eq. (2.28). When $\omega_w >> \omega_p$, the sum and difference frequency wave vectors $\vec{k}_+$ and $\vec{k}_-$ (see Fig. B.1) point in nearly the same direction, namely, the direction of $\vec{k}_w$ (the r-axis in Fig. 2.2). We may thus write $\Delta\eta_\pm = \Delta r_\pm$ and Eq. (B.9) becomes

$$\Delta r_{\pm} = \frac{2\pi/k_w}{\left(1 \pm \frac{k_p}{k_w}\right) - \sqrt{1 \pm 2\frac{k_p}{k_w}\cos\theta + \frac{k_p^2}{k_w^2}}} \quad . \tag{B.10}$$

Expanding the square root in the denominator and retaining only terms that are linear in k_p/k_w, we obtain

$$\Delta r_{\pm} = \frac{2\pi}{k_p(1 - \cos\theta)} \quad . \tag{B.11}$$

Equation (B.11) and Eq. (2.28) are identical. Thus the two methods yield equivalent results whenever $\omega_w >> \omega_p$.

REFERENCES

1. David T. Blackstock, "Propagation of plane sound waves of finite amplitude in nondissipative fluids," J. Acoust. Soc. Am. 34, 9-30 (1962).

2. David T. Blackstock, "Nonlinear Acoustics (Theoretical)," in American Institute of Physics Handbook, 3rd ed., Dwight E. Gray, ed. (McGraw-Hill Book Co., Inc., New York, 1972), pp. 3-183 to 3-205.

3. A.L. Thuras, R.T. Jenkins, and H.T. O'Neil, "Extraneous frequencies generated in air carrying intense sound waves," J. Acoust. Soc. Am. 6, 173-175 (1935).

4. H. Mrass and K. Brinkmann, "Phasenmodulation einer Ultraschallwelle in Luft, verursacht durch die Einwirkung einer zweiten Schallwelle," Acustica 14, 205-211 (1964). English translation available as "Phase modulation of an ultrasonic wave in air affected by the influence of a second sound wave," Technical Memorandum ARL-TM-76-5, Applied Research Laboratories, The University of Texas at Austin (1976).

5. Uno Ingard and David C. Pridmore-Brown, "Scattering of sound by sound," J. Acoust. Soc. Am. 28, 367-369 (1956).

6. H.O. Berktay and C.A. Al-Temimi, "Virtual arrays for underwater reception," J. Sound Vib. 9, 295-307 (1969).

7. H.O. Berktay and C.A. Al-Temimi, "Up-converter parametric amplifications of acoustic waves in liquids," J. Sound Vib. 13, 67-88 (1970).

8. W.L. Konrad, R.H. Mellen, and M.B. Moffett, "Parametric sonar receiving experiments," Naval Underwater Systems Center, Technical Memorandum PA4-304-71 (9 December 1971).

9. G.R. Barnard, J.G. Willette, J.J. Truchard, and J.A. Shooter, "Parametric acoustic receiving array," J. Acoust. Soc. Am. 52, 1437-1441 (1972).

10. James J. Truchard, "A theoretical and experimental investigation of the parametric acoustic receiving array," Technical Report ARL-TR-74-17, Applied Research Laboratories, The University of Texas at Austin, May 1974 (AD 783 099).

11. Hikaru Date and Yoshinori Tozuka, "Parametric directional microphone," D-4-6, Proceedings of the Sixth International Congress on Acoustics, Tokyo, Japan, August 1968, pp. D-125 to D-128.

12. J.J. Truchard (personal communication to D.T. Blackstock), 1977.

13. V.A. Zverev and A.I. Kalachev, "Modulation of sound by sound in the intersection of sound waves," Sov. Phys.-Acoust. 16, 204-208 (1970).

14. Robert D. Essert, Jr., "Axisymmetric propagation of a spherical N wave in a cylindrical tube," Technical Report ARL-TR-81-22, Applied Research Laboratories, The University of Texas at Austin, 4 May 1981 (ADA 099 990).

15. I. Rudnick (personal communication to D.T. Blackstock), 1980.

16. Leonid Pimonow, "Modulation d'ondes stationnaires ultra-sonores dans l'air," Annales des Telecommunications, Cahiers d'Acoustique 61, 24-28 (1954).

17. Robert T. Beyer, Nonlinear Acoustics (Naval Sea Systems Command, Washington, D.C., 1975).

18. G.D. Mikhailov, "The interaction of ultrasonic waves in liquids (in Russian)," Doklady Akad. Nauk. SSSR 89, 663-664 (1953).

19. A.G. Gorelik and V.A. Zverev, "On the problem of mutual interaction between sound waves," Sov. Phys.-Acoust. 1, 353-357 (1957).

20. V.A. Zverev and A.I. Kalachev, "Measurement of the interaction of sound waves in liquids," Sov. Phys.-Acoust. 4, 331-335 (1959).

21. J.M. Rouvaen, E. Bridoux, M. Moriamez, and R. Torguet, "Modulation of hypersound by ultrasound via strong collinear interaction," Appl. Phys. Lett. 23, 499-501 (1973).

22. E.T. Aksenov and A.S. Sherbakov, "Acoustooptic correlator based on collinear nonlinear interaction of elastic waves in a lead molybdate crystal," Sov. Tech. Phys. Lett. 6, 8-9 (1980).

23. D.H. Trivett and Peter H. Rogers, "Scattering of a cw plane wave by a pulse," J. Acoust. Soc. Am. 71, 1114-1117 (1982).

24. Peter J. Westervelt, "The nonscattering of sound by sound," J. Acoust. Soc. Am. 73, S82(A) (1983).

25. Peter J. Westervelt, "Parametric end-fire array," J. Acoust. Soc. Am. 32, 934-935(A) (1960). Also see "Parametric acoustic array," J. Acoust. Soc. Am. 35, 535-537 (1963).

26. Peter J. Westervelt, "Absorption of sound by sound," J. Acoust. Soc. Am. 53, 384(A) (1973).

27. Francis Hugh Fenlon, "An extension of the Bessel-Fubini series for a multiple frequency cw acoustic source of finite-amplitude," J. Acoust. Soc. Am. 51, 284-289 (1972).

28. Mark B. Moffett, William L. Konrad, and Lynn F. Carlton, "Experimental demonstration of the absorption of sound by sound in water," J. Acoust. Soc. Am. 63, 1048-1051 (1978).

29. Mark E. Schaffer, "The suppression of sound with sound," Technical Report ARL-TR-75-64, Applied Research Laboratories, The University of Texas at Austin, December 1975 (ADA 023 128).

30. Gong Xiu-fen, Zhu Zhe-min, and Du Gong-huan, "Nonlinear interaction of a finite-amplitude wave with a small-signal wave in air (in Chinese)," Journal of Nanjing University 76, 19-28 (1979). See also J. Acoust. Soc. Am. 65, S96(A) (1979).

31. William L. Willshire, Jr., "The suppression of sound by sound of higher frequency," Technical Report ARL-TR-77-22, Applied Research Laboratories, The University of Texas at Austin, May 1977 (ADA 040 008).

32. Roger G. Pridham, "A simple model for describing the interaction of infinitesimal and finite-amplitude waves," J. Acoust. Soc. Am. 55, S50(A) (1974).

33. V.A. Krasil'nikov, O.V. Rudenko, and A.S. Chirkin, "Absorption of low-amplitude sound due to interaction with noise," Sov. Phys.-Acoust. 21, 80-81 (1975).

34. V.I. Pavlov, "Sound absorption in a noisy medium," Sov. Phys.-Acoust. 22, 322-325 (1976).

35. T. Stanton and R.T. Beyer, "Interaction of sound with noise," J. Acoust. Soc. Am. 61, S14(A) (1977).

36. Don A. Webster and David T. Blackstock, "Collinear interaction of noise with a finite-amplitude tone," J. Acoust. Soc. Am. 63, 687-693 (1978).

37. S.N. Gurbatov, "Transformation of the statistical characteristics of noise in interaction with a strong regular wave," Sov. Phys.-Acoust. 27, 475-480 (1981).

38. M.F. Hamilton (personal communication), 1982.

39. Philip M. Morse and K. Uno Ingard, Theoretical Acoustics (McGraw-Hill Book Co., Inc., New York, 1968).

40. Sir Horace Lamb, Hydrodynamics, republication of the 6th ed., Cambridge University Press, 1932 (Dover Publications, Inc., New York, 1945).

41. D.E. Weston, "The theory of the propagation of plane sound waves in tubes," Proc. Phys. Soc. (London) B-66, 695-709 (1953).

42. Frederick M. Pestorius, "Propagation of plane acoustic noise of finite amplitude," Technical Report ARL-TR-73-23, Applied Research Laboratories, The University of Texas at Austin, August 1973 (AD 778 868), pp. 55-57.

43. H.E. Hartig and R.F. Lambert, "Attenuation in a rectangular slotted tube of (1,0) transverse acoustic waves," J. Acoust. Soc. Am. 22, 42-47 (1950).

44. B.P. Bogert, "Classical viscosity in tubes and cavities of large dimensions," J. Acoust. Soc. Am. 22, 432-437 (1950).

45. Ralph E. Beatty, Jr., "Boundary layer attenuation of higher order modes in rectangular and circular tubes," J. Acoust. Soc. Am. 22, 850-854 (1950).

46. E.A.G. Shaw, "Attenuation of (1,0) 'transverse' acoustic waves in a rectangular tube," J. Acoust. Soc. Am. 22, 512 (1950).

47. Philip M. Morse, Vibration and Sound (American Institute of Physics for the Acoustical Society of America, New York, 1976).

48. Stephen H. Burns, "Rational design of matched absorbing terminations for tubes," J. Acoust. Soc. Am. 49, 1693-1697 (1971).

49. A.M. Ghabrial, "Attenuation of the (1,0) and (2,0) modes in rectangular ducts," Acustica 5, 187-192 (1955).

50. P.E. Doak, "Excitation, transmission and radiation of sound from source distributions in hard-walled ducts of finite length (I): the effects of duct cross-section geometry and source distribution space-time pattern," J. Sound Vib. 31, 1-72 (1973).

51. P. Mariens, "Kirchhoff-Helmholtz absorption in wide and in capillary tubes at audible frequencies," J. Acoust. Soc. Am. 29, 442-445 (1957).

52. A. Said, "Modenfilter für Schallmessung im recteckigen Kanal," Acustica 50, 51-56 (1982).

53. Mark F. Hamilton, "Parametric acoustic array formation via weak collinear and noncollinear interaction in dispersive fluids," Technical Report ARL-TR-83-19, Applied Research Laboratories, The University of Texas at Austin, June 1983 (ADA 130 533).

54. Peter J. Westervelt, "Scattering of sound by sound," J. Acoust. Soc. Am. 29, 199-203 (1957).

55. V.A. Zverev and A.I. Kalachev, "Sound radiation from the region of interaction of two sound beams," Sov. Phys.-Acoust. 15, 322-327 (1970).

June 1984

DISTRIBUTION LIST FOR
ARL-TR-84-16
under Contract N00014-75-C-0867

Copy No.

1 Office of Naval Research
Physics Division Office (Code 412)
800 North Quincy Street
Arlington, VA 22217
Attn: L. E. Hargrove

2-13 Defense Technical Information Center
Cameron Station, Building 5
5010 Duke Street
Alexandria, VA 22314

14 Naval Research Laboratory
Department of the Navy
Washington, DC 20375
Attn: Technical Library

15-18 Naval Underwater Systems Center
New London Laboratory Detachment
New London, CT 06320
Attn: Technical Center
L. F. Carlton
W. L. Konrad
M. B. Moffett

19 NASA Langley Research Center
Mail Stop 460A
Hampton, VA 23665
Attn: W. L. Willshire

20-21 Naval Ocean Systems Center
San Diego, CA 92152
Attn: J. C. Lockwood
F. M. Pestorius

22-25 Naval Postgraduate School
Monterey, CA 93940
Attn: Technical Library
A. B. Coppens
S. L. Garrett
S. W. Yoon

Copy No.

26 Naval Research Laboratory
P. O. Box 8337
Orlando, FL 32856
Attn: A. L. Van Buren

27 Naval Coastal Systems Center
Panama City, FL 32407
Attn: D. H. Trivett

28 U.S. Naval Academy
Department of Physics
Annapolis, MD 21402
Attn: M. S. Korman

29-30 Brown University
Department of Physics
Providence, RI 02912
Attn: R. T. Beyer
P. J. Westervelt

31 University of California
Lawrence Livermore Laboratory
Theoretical Physics, L-71
P. O. Box 808
Livermore, CA 94550
Attn: S. I. Warshaw

32 University of California
at Los Angeles
Physics Department
Los Angeles, CA 90024
Attn: I. Rudnick

33-34 Calvin College
Grand Rapids, MI 49506
Attn: Physics Dept./R. D. Griffioen
Engineering Dept./J. P. Bosscher

35 Catholic University of America
Mechanical Engineering Department
Washington, DC 20064
Attn: J. A. Clark

36 Georgetown University
Physics Department
Washington, DC 20057
Attn: W. G. Mayer

37-39 Georgia Institute of Technology
School of Mechanical Engineering
Atlanta, GA 30332
Attn: J. H. Ginsberg
A. D. Pierce
P. H. Rogers

40 University of Houston/Central Campus
Cullen College of Engineering
Houston, TX 77004
Attn: B. D. Cook

41 Kalamazoo College
Department of Physics
Kalamazoo, MI 49007
Attn: W. M. Wright

42 Massachusetts Institute of
Technology
Mechanical Engineering Dept.
Room 31-159
Cambridge, MA 02139
Attn: M. A. Theobald

43 University of Mississippi
Physics Department
University, MS 38677
Attn: H. E. Bass

44 The Pennsylvania State University
Noise Control Laboratory
University Park, PA 16802
Attn: O. H. McDaniel

45 Rutgers University
Department of Mechanical Engineering
New Brunswick, NJ 08903
Attn: S. Temkin

46 University of Tennessee
Department of Physics
Knoxville, TN 37916
Attn: M. A. Breazeale

47 The University of Texas at Austin
Electrical Engineering Dept.
Austin, TX 78712
Attn: E. L. Hixson

48 Virginia Polytechnic and
State University
Engineering Science and Mechanics
Blacksburg, VA 24061
Attn: M. S. Cramer

49 Yale University
Department of Engineering
Mason Laboratory
9 Mill House Avenue
New Haven, CT 06520
Attn: R. E. Apfel

50 SOHIO Research Center
4440 Warrensville Center Road
Cleveland, OH 44128
Attn: W. N. Cobb

51-52 JBL, Inc.
P. O. Box 2200
8500 Balboa Blvd.
Northridge, CA 91329
Attn: Fancher Murray
J. S. McLean

53 Jet Propulsion Laboratory
4800 Oak Grove
Pasadena, CA 91103
Attn: T. G. Wang

54 Raytheon Co.
P. O. Box 360
Portsmouth, RI 02871
Attn: R. D. Pridham

55 Atlas Air Conditioning Company
5420 Gulfton
Houston, TX 77081
Attn: M. E. Schaffer

56 National Instruments
8900 Shoal Creek Blvd.
Austin, TX 78758
Attn: J. J. Truchard

57 Pyramid Technology
1295 Charleston Road
Mountain View, CA 94043
Attn: T. Van Baak

58 Artec Consultants, Inc.
245 7th Avenue/8th Floor
New York, NY 10001
Attn: R. D. Essert, Jr.

59 Nelson Industries, Inc.
Box 428
Stoughton, WI 53589
Attn: L. J. Eriksson

60-61 Hoover, Keith, and Bruce, Inc.
11381 Meadowglen
Suite I
Houston, TX 77036
Attn: Technical Library
H. L. Kuntz

62 T. L. Riley
2402 Harrowden
Austin, TX 78727

63 W. J. Hadden
J-Had Acoustics
2400 Westover
Austin, TX 78756

64 L. B. Orenstein-Crosse
6832A Hyde Park Drive
San Diego, CA 92119

65 Chief
Defence Research Establishment
Atlantic
Attn: H. M. Merklinger
P. O. Box 1012
Dartmouth, Nova Scotia
CANADA

66 University of Toronto
Institute for Aerospace Studies
Attn: W. G. Richarz
4925 Dufferin St.
Downsview, ON M3H 5TC
CANADA

67 Technical University of Denmark
Industrial Acoustics Laboratory
Attn: L. Bjørnø
Building 352
DK-2800 Lyngby
DENMARK

68 University of Bath
School of Physics
Attn: H. O. Berktay
Claverton Down
Bath BA2 7AY
ENGLAND

69 University of Leeds
Applied Math. Studies
Attn: D. G. Crighton
Leeds, Yorkshire LS2 9JT
ENGLAND

70 Institute of Sound
and Vibration Research
Attn: C. L. Morfey
The University
Southampton SO9 5NH
ENGLAND

71 Groupe d'Etude et de Recherche
de Detection Sous-Marines
Le Brusc
Attn: B. Lucas
B.C.A.N. Toulon 83800
FRANCE

72 Physikalisch-Technische
Bundesanstalt (PTB)
Attn: K. Brinkmann
Abteilung 5
33 Braunschweig
Postfach 3345
GERMANY

73 Kyushu Institute of Design
Acoustic Engineering
Attn: H. Date
4-9-1 Shiobaru Minami
Fukuoka, 815
JAPAN

74 Nagoya University
Department of Electrical Engineering
Attn: T. Kamakura
Furo-Cho
Chikusa-Ku
Nagoya
JAPAN

75 Osaka University
The Institute of Scientific
and Industrial Research
Attn: A. Nakamura
8-1, Mihogaoka, Ibaraki
Osaka 567
JAPAN

76 Tokai University
Marine Science and Technology
Attn: Shigemi Saito
Oridu Schimizu
Shizuoka, 424
JAPAN

77 Yoshisha University
Department of Electronics
Attn: Y. Watanabe
Kyoto, 602
JAPAN

78 Instituto de Acústica
Laboratorio de Ultrasonidos
Consejo Superior de Investigaciones
Científicas
Attn: J. A. Gallego-Juárez
Serrano, 144
Madrid-6
SPAIN

79 Universitet I Bergen
Matematisk Institutt
Attn: Sigve Tjøtta and
Jacqueline Naze Tjøtta
Allegaten 53-55
5000 Bergen
NORWAY

ARL:UT

80 ARL Library

81 A. Bedford

82 M. B. Bennett

83 Y. H. Berthelot

84 D. T. Blackstock

85 I. Busch-Vishniac

86 F. D. Cotaras

86 R. D. Costley

87 C. R. Culbertson

89 J. M. Estes

90 M. F. Hamilton

91 J. A. Hawkins

92 J. M. Huckabay

93 S. H. Kim

94 T. G. Muir

95 J. C. Navarro

96 D. A. Nelson

97-106 Nonlinear Acoustics Reserve

107 M. C. Penland-De Garcia

108-117 J. A. Ten Cate

118 E. A. Tschoepe

119 A. J. Tucker

END

FILMED

DTIC

END

FILMED

9-81

DTIC